Multiple-Input/Multiple-Output Characteristics of Piezo Devices and Their Applications

YOSHIDA, Tomoya / 吉田, 智哉

(開始ページ / Start Page)
1
(終了ページ / End Page)
74
(発行年 / Year)
2018-03-24
(学位授与番号 / Degree Number)
32675甲第427号
(学位授与年月日 / Date of Granted)
2018-03-24
(学位名 / Degree Name)
博士(工学)
(学位授与機関 / Degree Grantor)
法政大学 (Hosei University)
(URL)
https://doi.org/10.15002/00014765

Multiple-Input/Multiple-Output Characteristics of Piezo Devices and Their Applications

Tomoya YOSHIDA

CONTENTS

1. INTRODUCTION

The piezoelectric effect is the ability of certain materials to generate an electric charge in response to applied mechanical stress, and inversely to generate mechanical strain in response to electric voltage supply. This mutual characteristic of mechanical – electrical relations has been referred to as “reversibility”.

A variety of devices have been invented and manufactured based on this effect. Buzzers and/or loud speakers, vibrators, ignitors, energy harvesters, vibration sensors, electric filters, electric oscillators, and voltage transformers are typical examples. However the electric devices above suffer from undesirable temperature drift noise due to the pyroelectric effect of the piezo device. The physical relations of the devices above include not only reversible mechanical – electrical relation, but also reversible current–voltage, voltage–voltage and temperature–voltage relations. In conventional analyses of piezoelectric devices, these relations are independently treated and no general model has been considered. For example, when they are used as an electric filter, the model is an equivalent electric circuit.

In this study, first we build a general feedback model which describes all the relations above including the reversibility based on the piezoelectric effect, the pyroelectric effect, electrostatics and dynamics. Second, based on this general model, we consider the possibility of devices which include conventional as well as novel applications.

As a novel application, we propose a new mask-type bio-sensor which detects respiration and pulsation. This bio-sensor uses the pyroelectric effect which transduces the temperature of hot air ventilated from mouth or nose to voltage as well as the piezo effect which transduces the mechanical pulsation movement to voltage. If the bio-signal shows abnormal symptoms, the device is conversely used as an alarm sound generator. Furthermore, we present a novel, acoustic, tube type level meter which detects the bulk and powder level in a tank. In the application, we use the device as a sound generator in combination with an acoustic tube.

In this thesis, the following, second chapter, entitled “Multi-Input/Multi-Output Characteristics of Piezo Devices, describes the general model of the piezo effect.” The third chapter, entitled as “Respirometer by a Piezo Device and its Application to Triage,” describes a respirometer. The forth chapter, entitled “Powder and Bulk Level Monitoring by an Acoustic Tube Method,” describes a level meter application, and final fifth concluding chapter summarizes each chapter.

2.Multiple-Input/Multiple-Output Characteristics of Piezo Devices

Abstract— The objective of this paper is to understand the characteristics of the phenomena in piezo devices in a better manner, and to demonstrate a novel application for triage. That is, we focus not only the piezo effect, but also the pyroelectric effect of devices which may expand the possibility of their application fields. To accomplish this, instead of the conventional equivalent electric circuit, we use a lumped-mass mathematical model of the device based on electrostatics and mechanics using a block diagram and transfer functions. The proposed model shows that the piezo device has internal feedback, indicating that it can function as a multiple-input/multiple-output sensor and/or actuator with reversible characteristics. These characteristics allow us to apply piezo devices to triage to detect the vital signs of heartbeat and respiration when the device is set inside a mask. We developed a simple and robust low-power, mask-type triage sensor that visualizes the respiration and heartbeat.

Index Terms—multiple-input/multiple-output, piezo, pyroelectric, reversibility, feedback, triage.

2.1 INTRODUCTION

Certain types of devices exhibit reversible characteristics, whereby the input to the device can act as the output and vice-versa. For example, electromagnetic motors function as electromagnetic generators, and piezoelectric actuators generate a voltage when a force is applied to them. Because these devices function as not only actuators but also as sensors, they have attractive applications. A sensor-less automatic feedback control using these inverse functions alternately, in a time-sharing manner, is one example of such applications [1]-[9]. In this paper, we investigate the characteristics of piezo devices in detail, in order to use them as multiple-input/multiple-output sensors.

Piezo devices are applied in a variety of fields as electronic filters, electronic oscillators, sound generators, acceleration sensors, vibration sensors and vibrators, igniters, etc., [10]. Among these applications, the most common use for these devices is as electronic filters; hence, piezo devices have been modelled using an electric circuit [11] in spite of the interaction between electrical, mechanical, and thermal phenomena in the device. An equivalent electric circuit consists of a capacitor connected in parallel with a series-connected circuit containing a capacitor, coil, and resistor. This standard approach shows only one aspect of the phenomena occurring in the device, which limits its true potential.

To show the true potential of piezo devices, we built a model based on the electrical–mechanical piezo effect and the thermal–electrical pyroelectric effect. This model shows that reversibility is one aspect of the internal feedback in the device which functions as multiple-input/multiple-output sensor. Applying this model, we designed a triage sensor device set in a mask, which detects the heartbeat using the piezo effect and respiration using the pyroelectric effect.

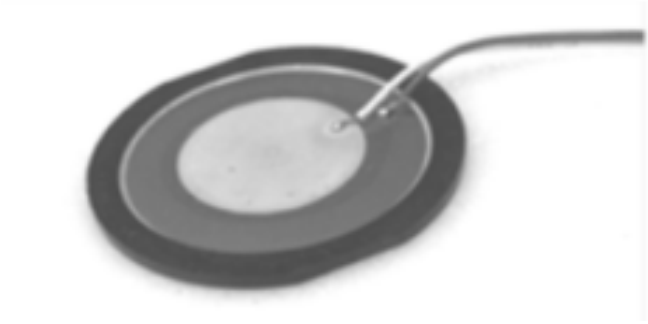

Fig. 1. Piezo device used in a buzzer.

2.2 PIEZO DEVICE FEEDBACK MODEL

A. Constants and variables of piezo devices

Figure 1 shows a piezo device used as a buzzer. When the device is pushed or bent, electric charges are generated and polarized. This generates a voltage between the front and rear electrodes. In contrast, when a voltage is applied between the electrodes, the Coulomb force expands or bends the electrodes. Assuming parallel-plate electrodes, we consider a lumped-mass model of the device in which the electrodes move perpendicularly to the plate surface. The constants and variables of the piezo device in Fig.1 are defined below.

[Constants]

<Electrical constants>

S: cross sectional area of electrode plate

d: gap between electrode plates

ε: dielectric constant of piezo material

Q: permanent electric charge in piezo material because of residual polarization

C: capacitance

<Mechanical constants>

m: mass of movable part of plate

D: damping coefficient of plate

k: stiffness constant of plate

<Thermal constant>

K: pyroelectric constant of piezo material

T_c: thermal time constant of heat radiation

[Variables]

<General variable>

t: time

<Electrical variables>

$e(t)$: input voltage

$E(t)$: total voltage by input voltage and piezo effect voltage

$q(t)$: electric charge generated by adding strain or polarized by feeding voltage between electrodes

$q_T(t)$: electric charge both by $q(t)$ and pyroelectric effect

$i(t)$: electric current given by a time derivative of $q(t)$

<Mechanical variables>

$f(t)$: input force

$F(t)$: total output force because of input force and piezo effect force

$x(t)$: input displacement

$X(t)$: total output displacement

< Thermal variables >

$T_a(t)$: atmospheric temperature at the rear electrode

$T_e(t)$: temperature at the front electrode

< Biological signals>

$E_h(t)$: heartbeat signal

$E_r(t)$: respiration signal

B. Modeling

The capacitance, internal voltage caused by the residual polarization, and static Coulomb force generated by the polarized electric charge balanced by stiffness of the plates are given as follows:

$$C = \frac{\epsilon S}{d},\ E = \frac{Q}{C} \text{ and } F = \frac{Q^2}{2\epsilon S} = \frac{Q}{2d}E \qquad (1)$$

When the piezo device plate is pushed by a force $f(t)$ and distorted, the gap between the electrodes reduces from d to $d-x(t)$, a polarized charge is generated which increases from Q to $Q+q(t)$, and the voltage between the electrodes increases from E to $E+e(t)$. From eq.(1), this situation can be described as follows:

$$Q + q(t) = \mathrm{CE} = \frac{\varepsilon S}{d - x(t)}E \approx \frac{\varepsilon S}{d}\left(1 + \frac{x(t)}{d}\right)E$$

$$= Q\left(1 + \frac{x(t)}{d}\right) = Q + \frac{Q}{d}x(t) \qquad (2a)$$

$$q(t) = \frac{Q}{d}x(t) \qquad (2b)$$

As the piezo device is made of a ferroelectric material, it is influenced by not only the piezo effect but also by the pyroelectric effect. Based on these two phenomena, piezo electric effect and pyroelectric effect, the electric charge between the electrodes can be described as follows:

$$q_T(t) = q(t) + K\Delta T(t) \qquad (3)$$

with the temperature difference between the front and rear electrodes being:

$$\Delta T(\mathrm{t}) = T_{\mathrm{a}}(t) - T_{\mathrm{e}}(t) \qquad (4a)$$

$$\frac{dT_{\mathrm{e}}(t)}{dt} = \frac{1}{T_{\mathrm{c}}}\Delta T(t) \qquad (4b)$$

The linear dependence of the temperature in certain ranges in eq.(4) by pyro effect has been investigated [10].

Furthermore, the relation between the force $F-f(t)$ and the electric charge $E+e(t)$ is given as follows:

$$F - f(t) = \frac{E+e(t)}{2d}Q = \frac{Q}{2d}E + \frac{Q}{2d}e(t) \qquad (5)$$

which yields:

$$f(t) = -\frac{1}{2}\frac{Q}{d}e(t) \qquad (6)$$

Thus, the equation of motion for the piezo material and electrode plates is described as follows:

$$m\frac{d^2x(t)}{dt^2} + D\frac{dx(t)}{dt} + kx(t) = f(t) \qquad (7)$$

The coefficient Q/d combines mechanical and electrical characteristics, and includes the dimension $[\mathrm{N/V}]$ or $[\mathrm{C/m}]$. The constant Q/d is referred to as the piezo constant that characterizes the device. In the equations presented above, the quantities are transduced from (displacement) - (charge) - (voltage) - (force) - (displacement), and constitute a feedback loop. Figure 2 presents the block diagram, which shows the internal signal flows in the piezo device. Any quantity in the feedback loop can be an input and/or an output of the device.

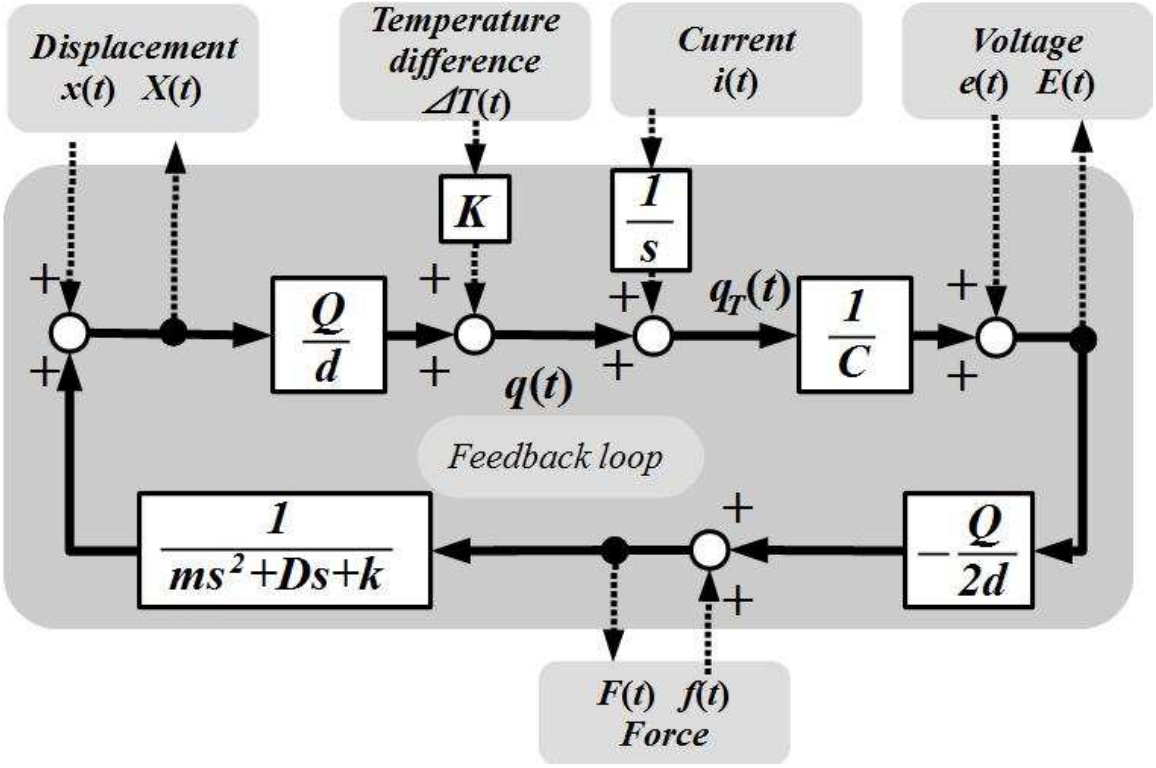

Fig. 2. Block diagram showing the internal feedback signal flows in the piezo device.

TABLE I TRANSFER FUNCTIONS OF THE OUTPUTS (FORCE, DISPLACEMENT, AND VOLTAGE) WITH RESPECT TO THE INPUTS (FORCE, DISPLACEMENT, VOLTAGE, TEMPERATURE, AND CURRENT)

Input \ Output	Force $F(s)$	Displacement $X(s)$	Voltage generation $E(s)$
Force $f(s)$	———	———	Changing force sensor
	$\frac{ms^2+Ds+k}{\Delta(s)}$	$\frac{1}{\Delta(s)}$	$\frac{Q}{Cd}\frac{1}{\Delta(s)}$
Displacement $x(s)$	Stiffener controller switch	———	Displacement sensor
	$\frac{-1}{2C}(\frac{Q}{d})^2\frac{ms^2+Ds+k}{\Delta(s)}$	$\frac{ms^2+Ds+k}{\Delta(s)}$	$\frac{Q}{Cd}\frac{ms^2+Ds+k}{\Delta(s)}$
Voltage $e(s)$	Actuator	Sound generator	Electrical filter
	$\frac{-Q}{2d}\frac{ms^2+Ds+k}{\Delta(s)}$	$\frac{Q}{Cd}\frac{1}{\Delta(s)}$	$\frac{ms^2+Ds+k}{\Delta(s)}$
Temperature difference $\Delta T(s)$	Thermal actuator	Thermal switch	Changing temperature sensor
	$\frac{-QK}{2Cd}\frac{ms^2+Ds+k}{\Delta(s)}$	$\frac{-QK}{2Cd}\frac{1}{\Delta(s)}$	$\frac{K}{C}\frac{ms^2+Ds+k}{\Delta(s)}$
Current $i(s)$	———	———	Impedance
	$\frac{-Q}{2Cds}\frac{ms^2+Ds+k}{\Delta(s)}$	$\frac{-Q}{2Cds}\frac{1}{\Delta(s)}$	$\frac{1}{Cs}\frac{ms^2+Ds+k}{\Delta(s)}$

Characteristic polynomial $\Delta(s)=ms^2+Ds+k+\frac{1}{2C}(\frac{Q}{d})^2$

Conventionally, the piezo device has been used as a device for voltage-input and displacement-output or force-output, as well as for displacement-input or force-input and voltage-output. However, as shown in Fig.2, the possible transfer functions of force, displacement, and voltage, with respect to force, displacement, voltage, temperature, and current can be considered as shown in Table 1

C. Piezo characteristics from the model

In order to show the validity of the model, we will compare the frequency responses of the theoretically calculated impedance and the experimentally measured impedance. Note that the impedance can be easily determined from the voltage and current. From Table I, the impedance is given as follows:

$$\mathrm{Z(s)} = \frac{e(s)}{i(s)} = \frac{1}{sC} \cdot \frac{ms^2+Ds+k}{ms^2+Ds+k+\frac{1}{2C}\left(\frac{Q}{d}\right)^2} \tag{8}$$

The theoretically estimated sketch for the frequency response is shown in Figure 3, and the anti-resonance frequency f_{ar} and the resonance frequency f_{r} are given as follows:

$$f_{\mathrm{ar}} = \frac{1}{2\pi}\sqrt{\frac{k}{m}}, \quad f_{\mathrm{r}} = \frac{1}{2\pi}\sqrt{\frac{k+\frac{1}{2C}\left(\frac{Q}{d}\right)^2}{m}} \tag{9}$$

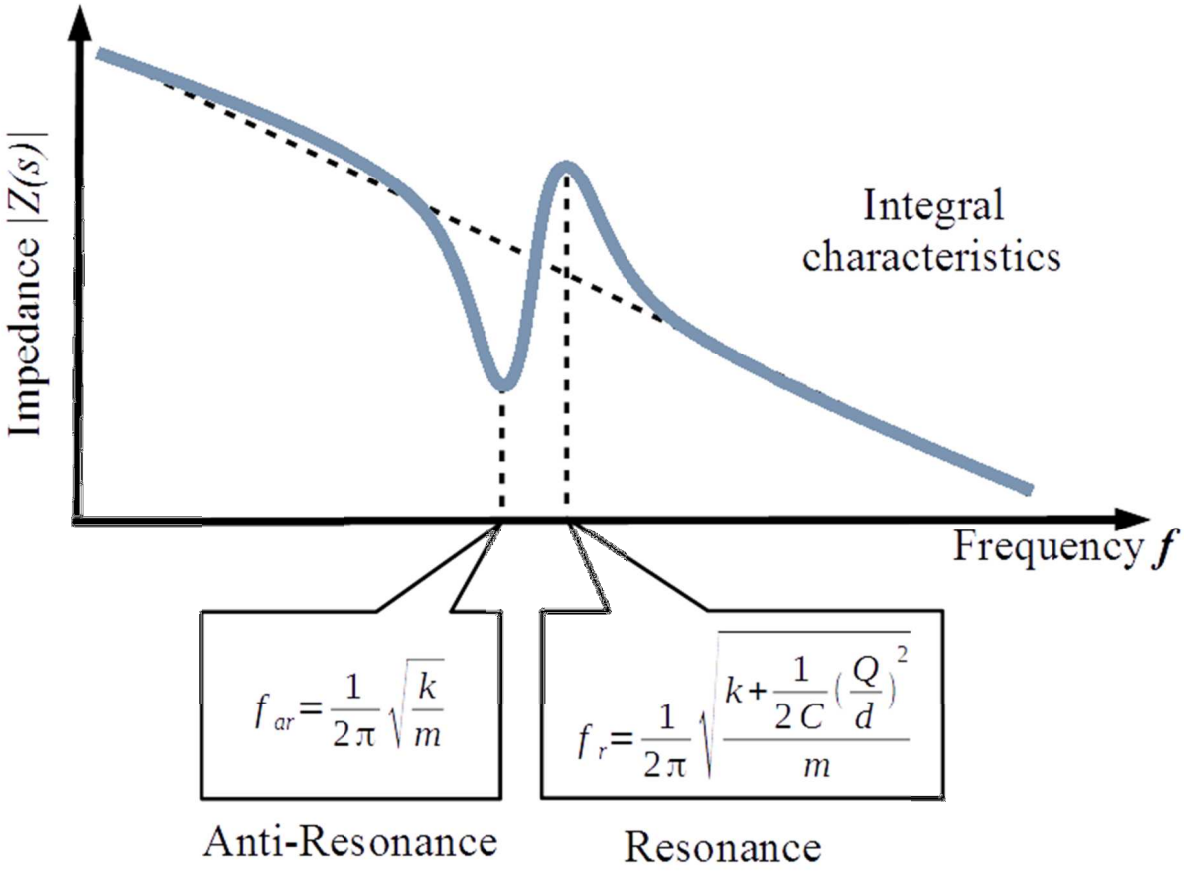

Fig. 3. Frequency response of impedance of the piezo device theoretically estimated from eq.(8). Single anti-resonance and single resonance frequencies exist.

From the frequencies f_{ar} and f_{r} in eq.(9), the stiffness constant k and piezo constant Q/d can be estimated as follows from f_{ar}, f_{r}, m, and C:

$$k = m(2\pi f_{\mathrm{ar}})^2, \quad \frac{Q}{d} = 2\pi\sqrt{2mC\left(f_{\mathrm{ar}}{}^2 - f_{\mathrm{r}}{}^2\right)} \tag{10}$$

D. Pyroelectric characteristics from the model

From Table I, the transfer function of the output voltage with respect to the change in temperature is given as follows:

$$\frac{E(s)}{T_e(s)} = \frac{K}{C} \cdot \frac{sT_c}{1+sT_c} \cdot \frac{ms^2+Ds+k}{ms^2+Ds+k+\frac{1}{2C}\left(\frac{Q}{d}\right)^2} \qquad (11)$$

This transfer function expresses the pyroelectric characteristics. Immediately after a temperature change, the transfer function can be approximated as follows from eq.(11) using the initial-value theorem of Laplace transform:

$$\frac{E(s)}{T_e(s)} = \frac{K}{C} \qquad (12)$$

2.3 CHARACTERISTICS OF PIEZO BUZZER DEVICE

In this section, we experimentally investigate the piezo and pyroelectric characteristics of the buzzer (PRIMO: DC-5DSN4) shown in Fig.1.

A. Piezo effect characteristics from the frequency response of impedance

First, we examine the piezo characteristics using the frequency response of impedance. From the specifications of the buzzer, the following parameters are obtained: resonance frequency: f_r=750±100[Hz], resonance impedance: 2[kΩ], capacitance: C=70[nF], maximum input voltage: 30[V_p−p], maximum acoustic pressure level: 75[dBspl], and insulation impedance: 10[MΩ]. Furthermore, we measured the following parameters: mass: m=0.001[kg], damping coefficient: D=0.25[N/(m/s)], stiffness constant: k =2.8×10⁴[N/m], piezo constant: Q/d=0.026[N/C] and/or [V/m], thickness of piezo device =5.0×10^{-5}[m] , and thickness of aluminum plate = 2.0×10^{-4}[m].

The impedance frequency response was measured using a network analyzer (Analog Discovery 2).

TABLE II shows the summarized specification of piezoelectric and mechanical properties of the PRIMO: DC -5DSN4 buzzer.

TABLE II SPECIFICAION OF THE BUZZER (PRIMO: DC -5DSN4) USED FOR EXPERIMENTS

Electrode plate	diameter	50[mm]
	thickness	0.2[mm]
	material	aluminum
Piezo	diameter	21[mm]
	thickness	0.05[mm]
	Thermal expansion coefficient	71×10^{-5} [1/℃]
	Piezo constant	0.026[N/C]or[V/m]
Device	mass	0.001kg
	stiffness	2.8×10^{4} [1/℃]
	Damping coefficient	0.25[N/(m/s)]
	capacitance	70[nF]
	Insulation impedance	10[MΩ]
	Maximum input voltage	30[V]
	Resonance frequency	750±100Hz
	Resonance impedance	2[kΩ]
	Maximum acoustic pressure level	75[dBspl]

Figure 4(a) shows the calculated frequency response from eq.(8), and Fig. 4(b) shows the experimentally measured response. Both show similar characteristics in the anti-resonance and resonance frequency ranges. In the low- and high-frequency ranges, the characteristics are different. In the low-frequency range, the impedance measured in the experiment is greater than that obtained from the calculations. In the high-frequency range, the frequency response from the experiment contains resonance and anti-resonance frequency components, whereas no resonance or anti-resonance frequency components are observed in the calculated results. This is because the model is a lumped-mass model with a single mass, damper, and plate spring.

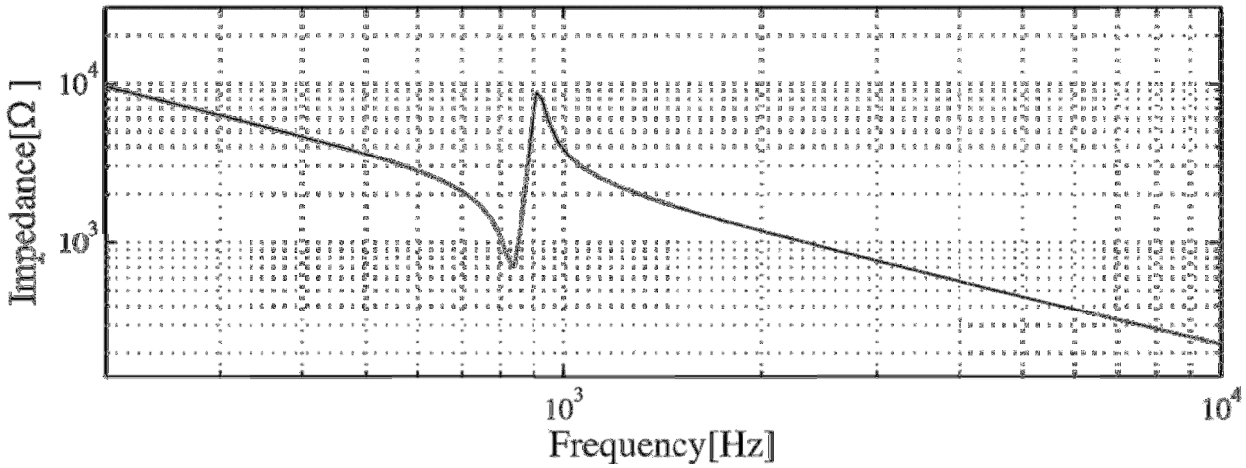

(a). Impedance frequency response of the device calculated using eq.(8). Single anti-resonance frequency and single resonance are observed.

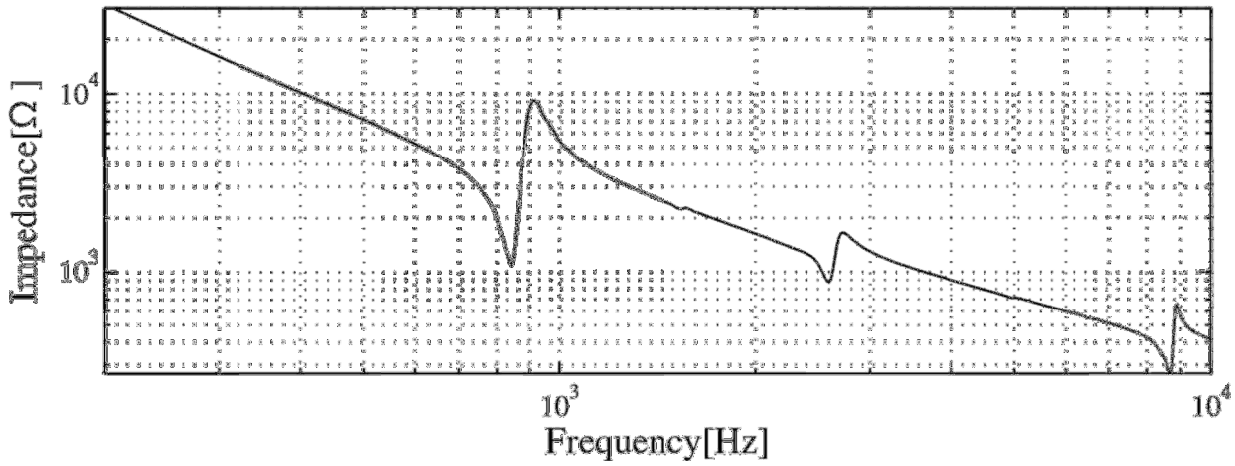

(b). Measured impedance frequency response from a spectrum analyzer. Fundamental anti-resonance and resonance, as well as higher-harmonic anti-resonance and resonance phenomena, are observed.

Fig. 4. Frequency response

B. Pyroelectric characteristics by thermal time response

Next, we examine the pyroelectric characteristics using the thermal time response. Figure 5 shows the experimental setup.

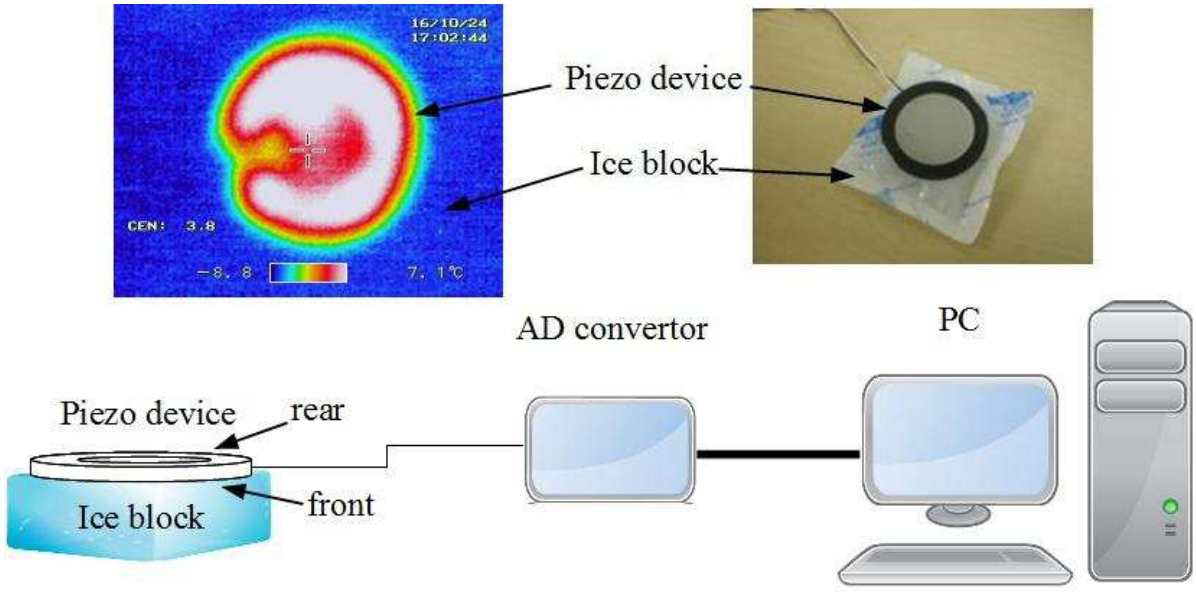

Fig. 5. Experimental setup to investigate the pyroelectric effect of the device. The device was silently but firmly placed on an ice block.

The output voltage was detected from the two electrodes through detecting copper wires as shown in Fig.1 and acquired directly from the device without amplification into the AD converter. As shown in Fig. 5, the front electrode was silently but firmly placed on an ice block at a stable temperature of 0 [℃] as a heat sink at time t = 0. The atmospheric room temperature was 26[℃]. The temperature of the front electrode decreased to around 10[℃] quickly. In addition, the temperature of the rear electrode that was exposed to atmosphere decreased to 14[℃] within 1 [s]. Thus, the temperature difference between the electrodes follows a step function with a magnitude of 4[℃]. No external force such as dynamic pressure by wind was exerted. We measured the time response of the output voltage as shown in Figure 6. In a previous paper, high temperature characterization of PZT(0.52/0.48) thin-film pressure sensors was investigated [13]. This research showed that despite the fluctuations in resonant frequency with increasing temperature, the proposed PZT sensor can be effectively used in high temperature/pressure applications. Compared to this study, the piezo device application in our paper operates under normal temperature/pressure levels and makes use of the pyroelectric effect of the device.

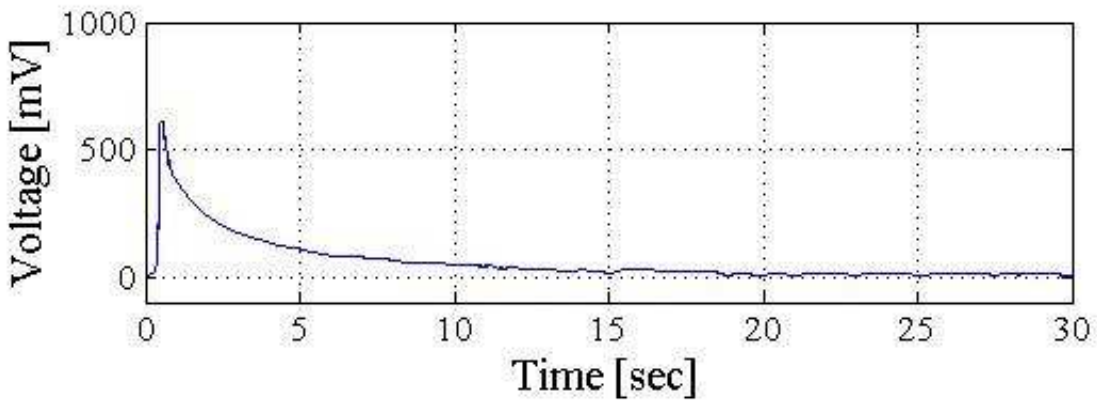

Fig. 6. Time response of output voltage when the temperature difference was changed in a step-function manner with a magnitude of 14[℃].

Immediately after the device was set on the ice block, the output voltage increased to approximately 600 [mV], and then decreased to zero. Based on the theoretical gain, immediately after the step change, given in eq.(12), we have

$$\frac{K}{C} = \frac{600[\text{mV}]}{14[℃]} = 43\left[\frac{\text{mV}}{℃}\right] \qquad (13)$$

Thus, the pyroelectric constant can be estimated as follows:

$$K = C \cdot (measured\ gain) = 70[\text{nF}] \times 43\left[\frac{\text{mV}}{℃}\right]$$

$$= 3010[\text{nC}/℃] \qquad (14)$$

Note that the output voltage may occur due to the thermal expansion of the piezo ceramic itself. As the thermal expansion coefficient of ceramic is $7.1 \times 10^{-6}[/℃]$ and the thickness of the piezo ceramic material is $5 \times 10^{-5}[\text{m}]$, the displacement of thermal expansion per degree is estimated as follows:

$$7.1 \times 10^{-6}[/℃] \times 5 \times 10^{-5}[\text{m}] \times 1[℃] = 3.55 \times 10^{-10}[\text{m}], \qquad (15)$$

which generates the steady-state voltage, from the transfer function of voltage with respect to displacement (given in Table I), as follows:

$$E = \frac{1}{C} \cdot \left(\frac{Q}{d}\right) \cdot \frac{k}{k + \frac{1}{2C}\left(\frac{Q}{d}\right)^2} \cdot \varepsilon = 0.11[\text{mV}] \qquad (16)$$

The increase in the voltage due to the pyroelectric effect is $43[\text{mV}/℃]$, whereas that due to the thermal expansion is calculated to be $0.11[\text{mV}/℃]$, which is negligibly smaller than the increase in voltage due to the pyroelectric effect.

C. Effect by dynamic pressure

Because the device is highly sensitive, it may be influenced by dynamic pressure from the patient's exhaled air. Here, we investigate how the device is influenced by the airflow. Figure 7 shows the experimental setup. A blower, which blows air at different temperatures, was set in front of the device. Note that the peak air-flow speed in normal human exhalation is 0.5[m/s] and the temperature is around 36[℃]; this condition is considered in our examinations. The 26[℃] room-temperature airflow at speeds ranging from 0.5[m/s] to 10.0[m/s], and the 36[℃] airflow at a speed of 0.5[m/s], were fed to the device. Figure 8(a) shows the output voltage when the 26[℃] airflow at a speed of 10[m/s] was used. In steady state condition, the output voltage is approximately 0[V], and its amplitude is 8.6[mV]. When airflow at the same temperature and 5.0[m/s] speed was used, the output voltage was again steady and the amplitude was 4.2[mV]. Similarly, when airflow with 0.5[m/s] speed was used, the amplitude was 3.0[mV]. Fig. 8(b) shows the output voltage when airflow at 36[℃] and 0.5[m/s] speed (human exhalation) was fed to the device. The noise in Fig.8(b) is mainly due to the turbulent flow from the blower. The output voltage suddenly increased to 743[mV] and gradually attenuated to 0[V].

These results show that output voltage change occurred not due to dynamic pressure but due to the temperature change in the device, which was caused by the pyroelectric effect.

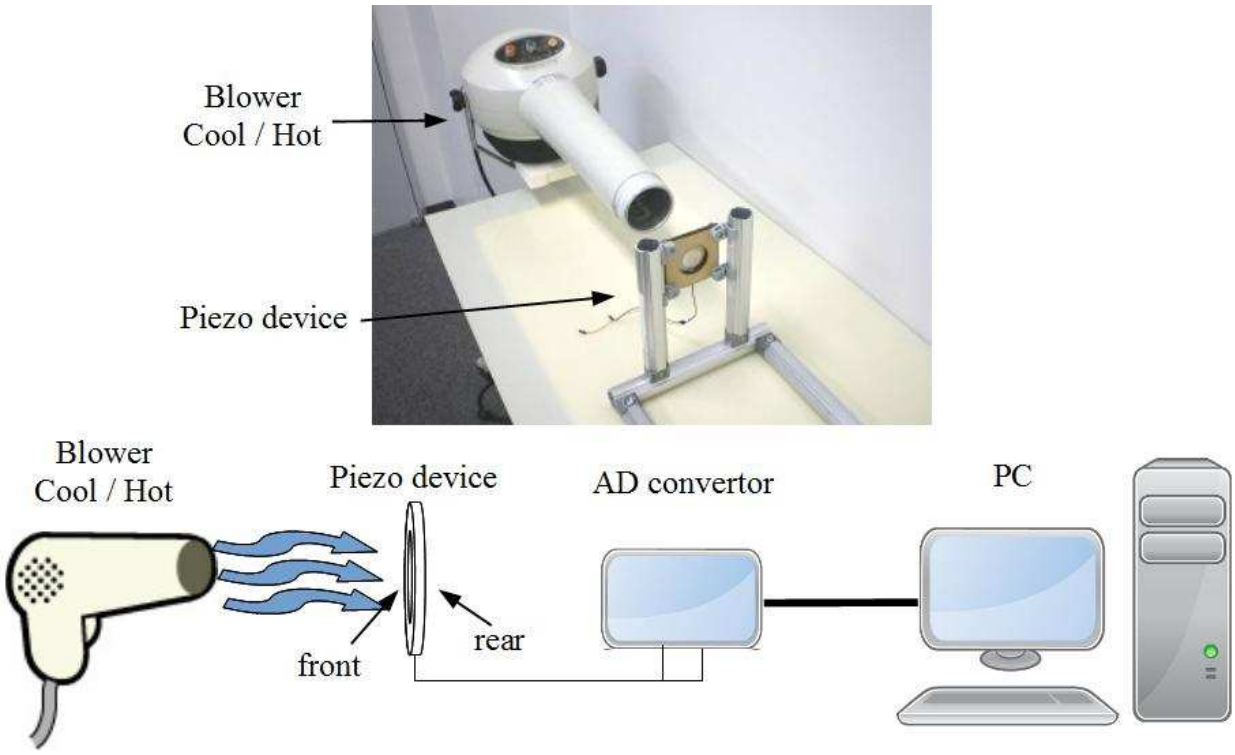

Fig.7 Experimental setup to investigate dynamic pressure due to airflow.

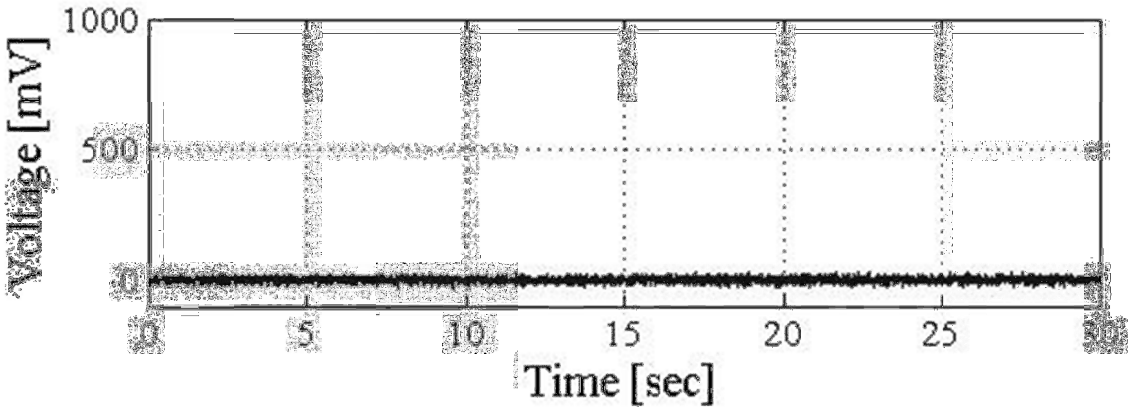

(a) Output voltages for airflow at 26[℃] (room temperature) and 10.0 [m/s] speed

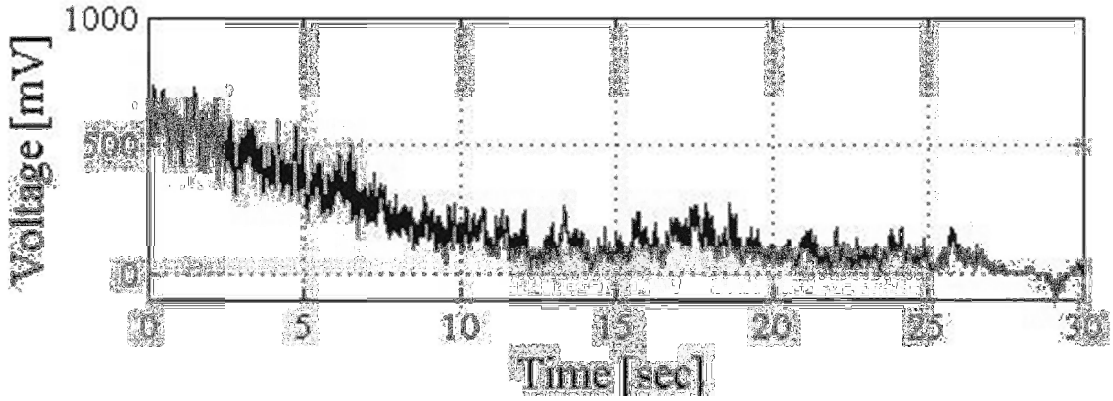

(b) Output voltages for airflow at 36[℃] (human body temperature) and 0.5 [m/s] speed

Fig.8 Output voltages for room-temperature and hot-temperature airflows.

2.4 APPLICATION IN TRIAGE

A. Triage

Among the variety of possible applications of piezo devices to health care, we chose to focus on triage. Serious natural disasters such as a major earthquakes, and tsunami or man-made disasters such as suicide bombings by terrorists leave many people injured at once, overwhelming hospitals which may not be able to provide sufficient medical care. After the Great East Japan Earthquake, the wounded lay on beds, couches, and even on the floor, in dark passages. Their conditions changed quickly over time and some died because of the lack of sufficient medical attention. Triage is a priority determination procedure which ensures proper assignment of the available resources in the most effective manner. It also helps in classifying the patients as: 0: DEAD (black card), I: IMMEDIATE (red card), II: DELAYED (yellow card), and III: MINOR (green card). The patients are cared for in order, from I to III. The simple triage and rapid treatment (referred to as START) is one of the standard methods used. Treatment priority is determined based on the flow chart in Figure 9. In this process, the bio-signals employed are: (1) visual inspection of ambulatory ability, (2) respiration, and (3) heartbeat.

Therefore, if both heartbeat and respiration could be detected automatically, it would be extremely useful in triage. Here, we propose a sensing device based on a piezo device, which can measure both heartbeat and respiration simultaneously.

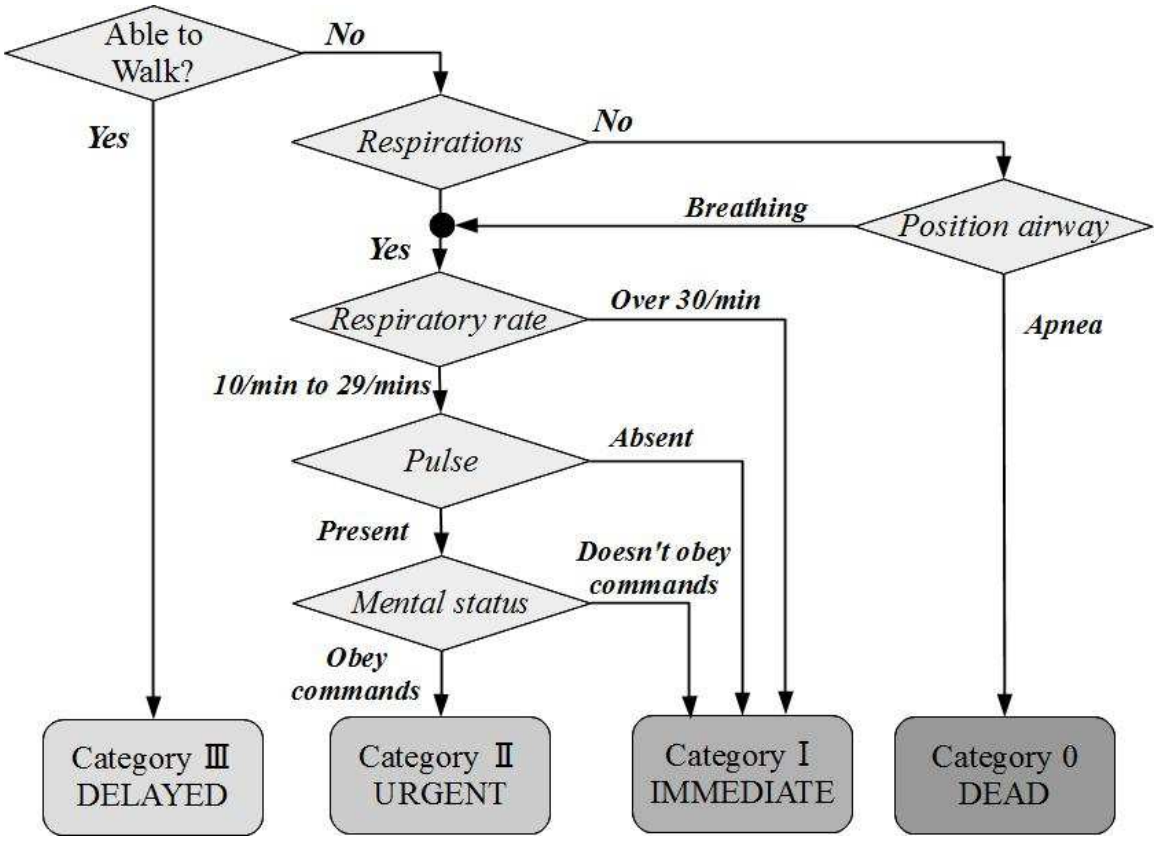

Fig. 9. The simple triage and rapid treatment (START) process.

B. Proposed System for Simultaneous Measurement of Heartbeat and Respiration

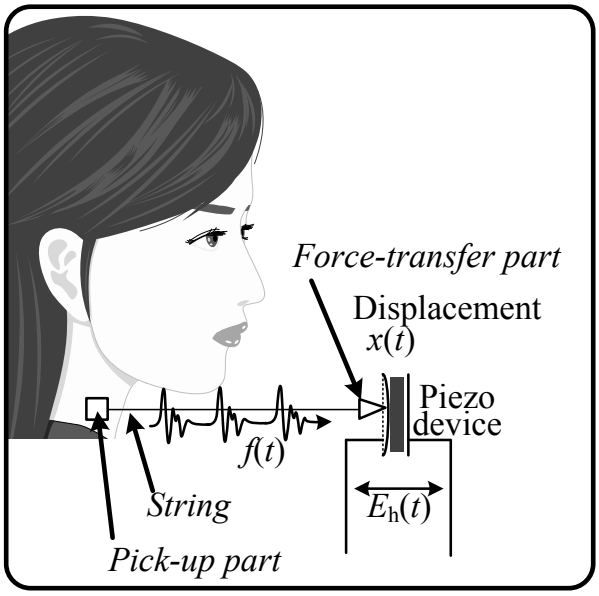

(a) Principle of the measurement for the heartbeat by the piezo device.

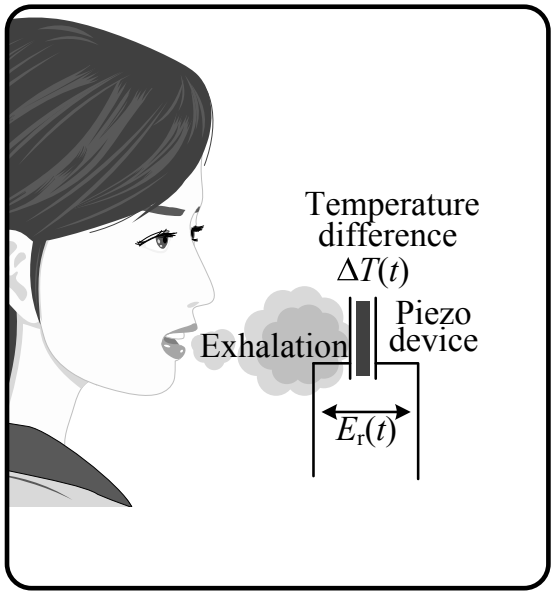

(b) Principle of the measurement for the respiration by the piezo device.

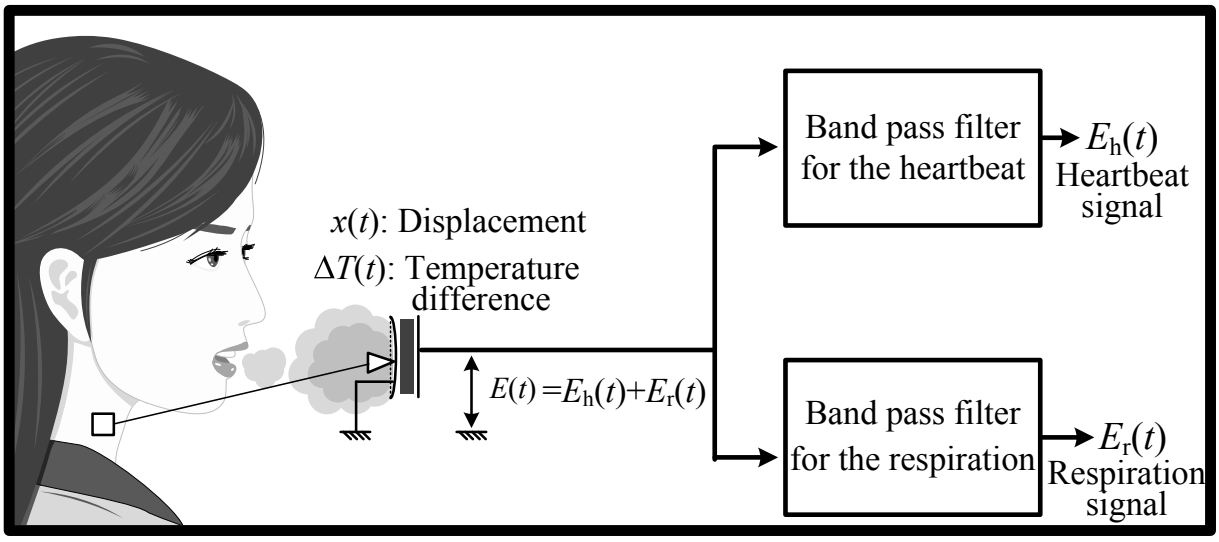

(c) Proposed system to measure the heartbeat and respiration signals for the triage by using a piezo device.

Fig. 10. Measurement principles for heartbeat and respiration using a piezo device.

Figure 10 (a) shows the measurement principles for detecting the heartbeat signal using a piezo device. A pick-up part is placed on the neck of the patient, pushing against the carotid. The force-transfer part is attached to a surface of the piezo device. The pick-up part and the force-transfer part are connected using a tense string. When the patient's blood flows periodically through the carotid, the vibrations $f(t)$ due to the blood flow push against the pick-up part, which in turn pushes the center of the piezo device through the string and the force-transfer part. As a

result of pushing the piezo device, a displacement $x(t)$ occurs in the piezo device. The piezo device generates a voltage $E_h(t)$ corresponding to $x(t)$, in synchronization with the pulsation, according to the transfer function of voltage with respect to force.

Fig. 10(b) shows the measurement principles used to detect the respiration signal using a piezo device. The exhaled hot air arrives at the piezo device when the patient breathes, and a temperature difference $\Delta T(t)$ occurs between the mouth side and other side of the device. The device generates a voltage $E_r(t)$ in accordance with the transfer function of voltage with respect to temperature.

Fig. 10(c) shows the proposed system to obtain heartbeat and respiration signals, simultaneously. Using both the vibration $f(t)$ due to the heartbeat and the temperature difference $\Delta T(t)$ due to respiration as the inputs to the piezo device, the output voltage $E(t)$ from the piezo device can be represented as a linear combination of the heartbeat signal $E_h(t)$ and the respiration signal $E_r(t)$. Hence, $E(t)$ is expressed as $E(t) = E_h(t) + E_r(t)$. $E_h(t)$ and $E_r(t)$ can be discriminated using bandpass filters.

C. Experimental Setup

Figure 11 shows a proposed mask-type triage sensor, which measures heartbeat and respiration based on the principle described in Fig. 10. The piezo device is set in the middle of a mask, and the piezo material is inside the mask so that the exhaled hot air arrives directly at the piezo device. The mask is attached firmly using rubber strings with tension. One string is placed around the head and the other around the neck. The rubber string around the neck runs through a styrofoam block which is set up to push the carotid as a pick-up part.

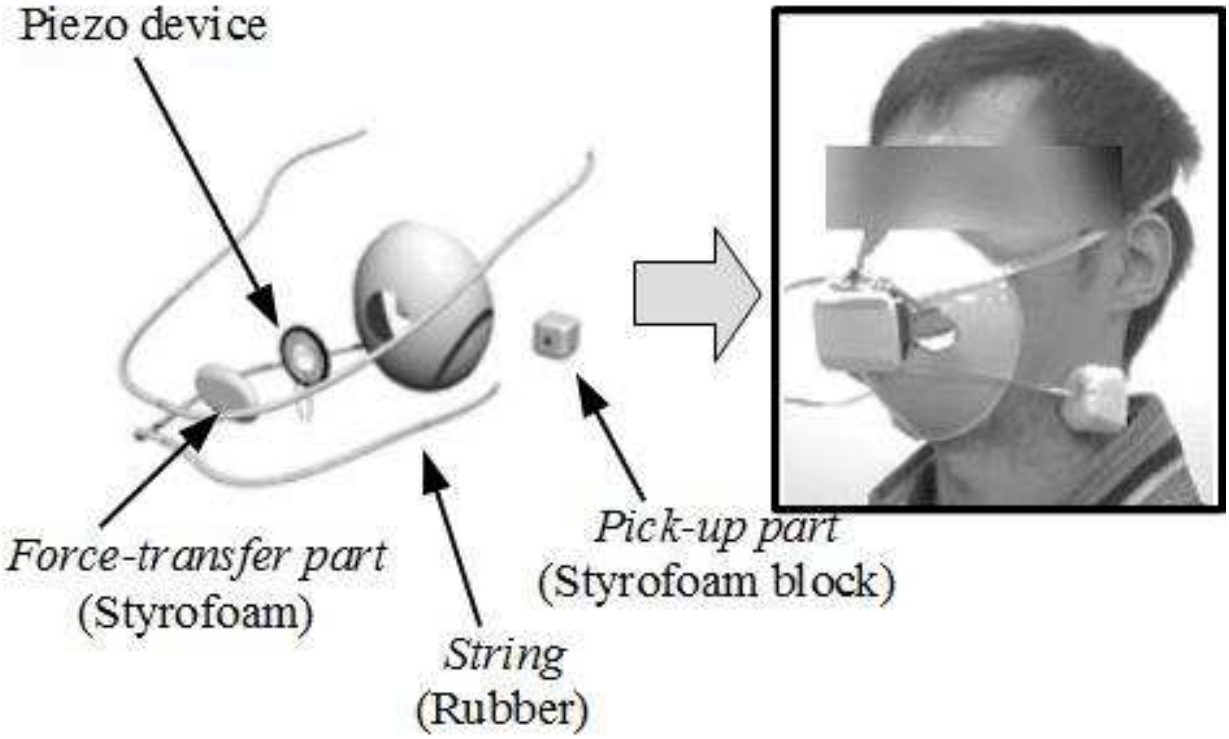

Fig. 11. System for simultaneous measurement of heartbeat and respiration.

Figure 12 shows the experimental setup using the proposed system. We also measured the heartbeat and respiration signals using a medical pulse sensor and a microphone-type respirometer, respectively, for comparison.

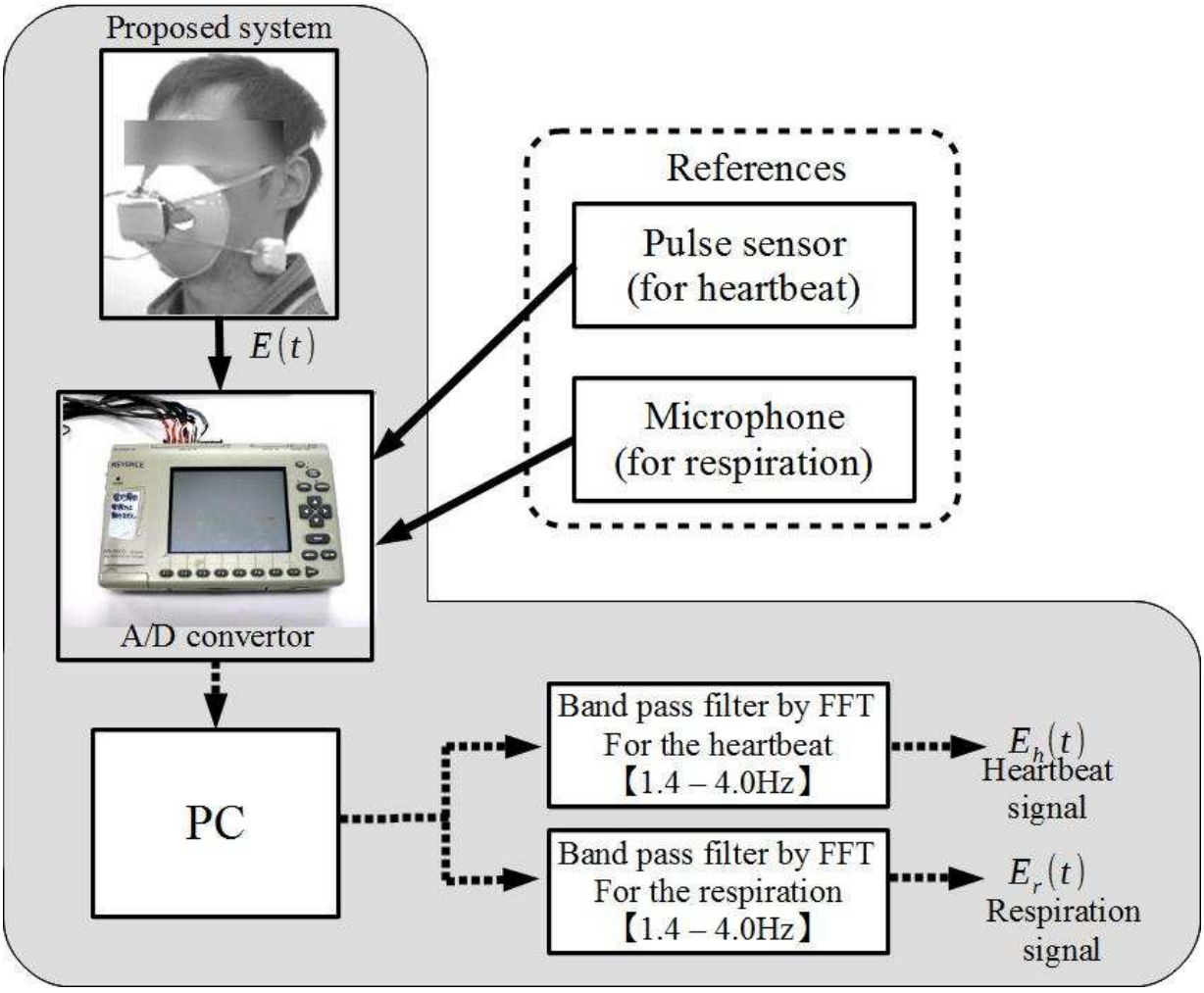

Fig. 12. Experimental setup and situation for measuring heartbeat and respiration using the system in Fig.10.

The output from the piezo device was directly connected to an AD converter, without using an amplifier, and transferred into a personal computer (OPTIPLEX 960). The voltage range of the AD converter (NR-2000) was set as ± 1.0[V] and the sampling interval was set to 1 [ms]. The signal acquired was digitally filtered using a non-recursive FFT method. A bandpass filter with a pass-band from 1.5[Hz] to 4.0[Hz] was employed to filter the heartbeat signal, and another filter with a passband from 0.1[Hz] to 1.4[Hz] was employed to filter the respiration signal.

D. Experimental Results

Figure 13 shows the output voltage $E(t)$ from the piezo device when it was set up as shown in Fig.12. In this case, the subject was breathing normally. The output voltage was not amplified. The respiration signal is conspicuous, but the heartbeat signal is weak.

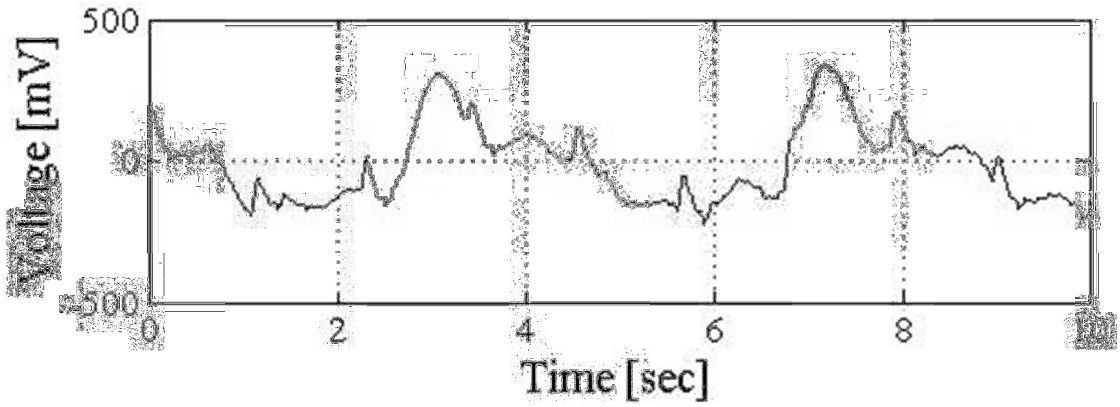

Fig. 13. Output voltage $E(t)$ from the piezo device without amplification in the situation shown in Fig. 12.

Figure 14 shows the digitally filtered heartbeat signal $E_h(t)$. The signal-to-noise (S/N) ratio was 39.2 [dB], where noise was defined by the standard deviation when the mask was set on the table and the signal was defined by the average of the peak to peak values of the heartbeat signal.

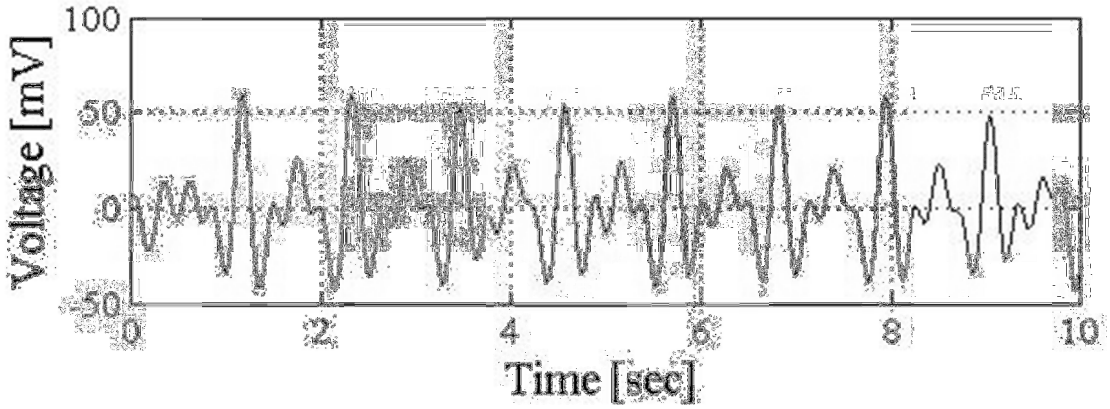

Fig. 14 Non-recursive digital bandpass filtered heartbeat signal $E_h(t)$ detected by the piezo device using the FFT method. The band was from 1.5[Hz] to 4.0[Hz]. The S/N ratio was 39.2[dB].

Figure 15 shows the two R-R intervals, which are the periods between the pulsations using the piezo device and the medical pulse sensor (SEN-11574) that measures the heart rate period.

The R-R interval measured by the piezo device fluctuates, but the average of over 10 [s] includes only a 5[%] error rate, which is allowed in triage applications [12].

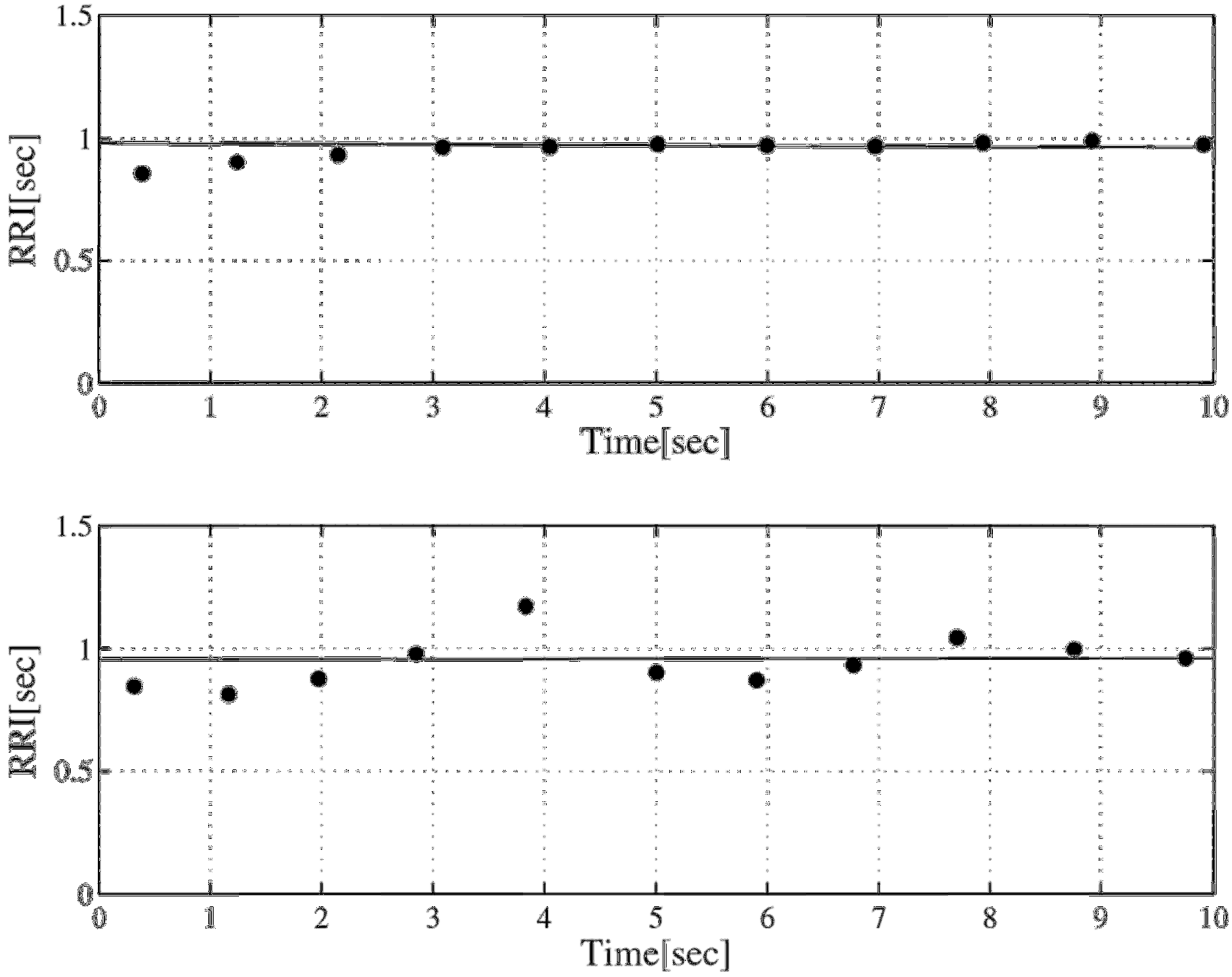

Fig. 15. R-R intervals: Upper plots are from the medical pulse sensor and lower plots are from the piezo device.

Figure 16 shows the respiration signal $E_r(t)$. The slow-changing signal is the respiration signal from the piezo device and the fast-changing signal is from the microphone-type respirometer. The data show that they are synchronized with each other. The S/N ratio was 55.6 [dB], where the noise level and signal level were defined in a manner similar to that used in measuring of the heartbeat signal. The output voltage of respiration is high. Thus even weak respiration can be detected.

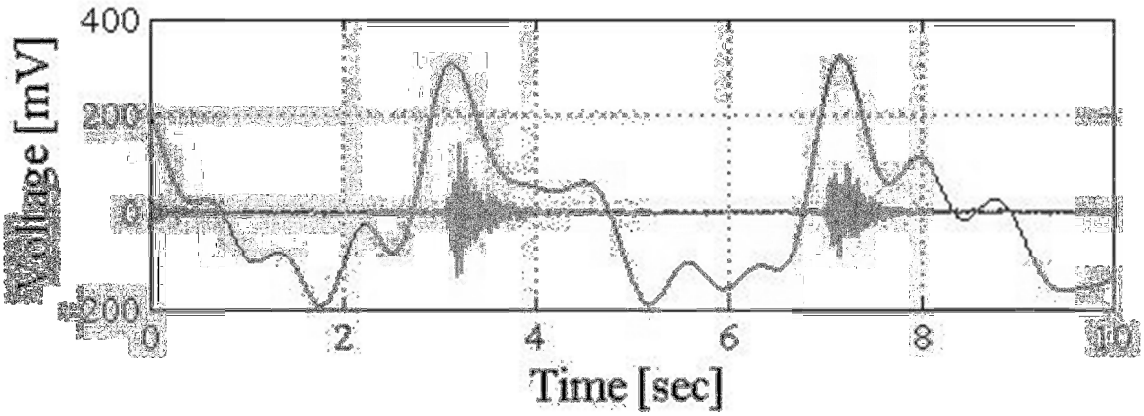

Fig. 16. Non-recursive digital bandpass filtered respiration signal $E_r(t)$ detected by the piezo device, and the respiration signal detected by the microphone-type respirometer. The band was from 0.1[Hz] to 1.4[Hz]. The S/N ratio was 55.6[dB].

E. Respiration sensor using a simple system

At a real disaster site, a robust and easily attachable measurement device is a prerequisite for any device. As a vital sign, respiration is essential as shown in the triage procedure flow chart (START) in Fig. 9. The first step is the visual inspection of the ambulatory ability, and the next check is for the presence of respiration. These two steps are conducted by medical staff with the patient lying on a bed. The third inspection is to count the number of breaths per minute, which can be conducted automatically using measurement devices that emit light or sound in an emergency. Here, we present a compact, battery-driven, low power consumption LED optical output device. Figure 17 shows the proposed simple and robust respiration measurement system.

In the circuit, we used a buzzer device (PRIMO: DC5DSN4), a high-luminance LED, and a button-type battery (CR2032). Energy consumption of the circuit is low and in standby condition, it can last for approximately three years. When used regularly, it works for around 20 [h].

Figure 18 shows how the proposed mask triage sensor are placed. The LED emits light synchronized with respiration. The light intensity is proportional to the strength of the breathing.

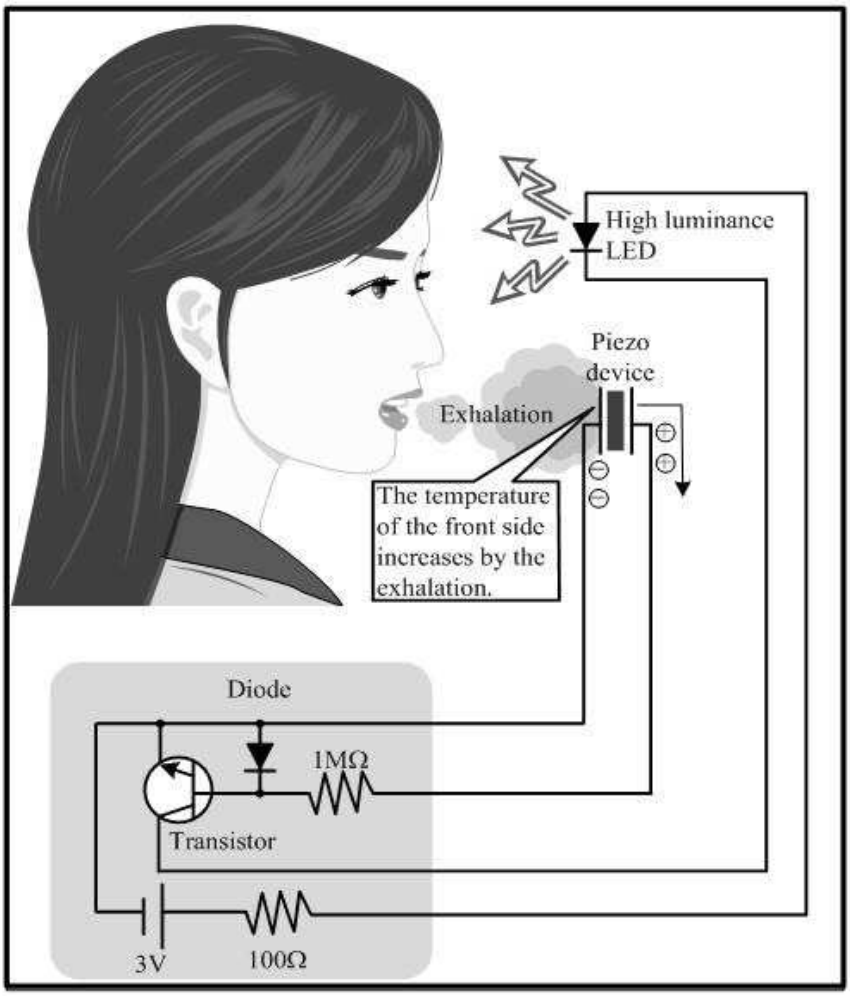

Fig. 17. Respiration detection using the pyroelectric effect of the piezo device, and the circuit for optical display.

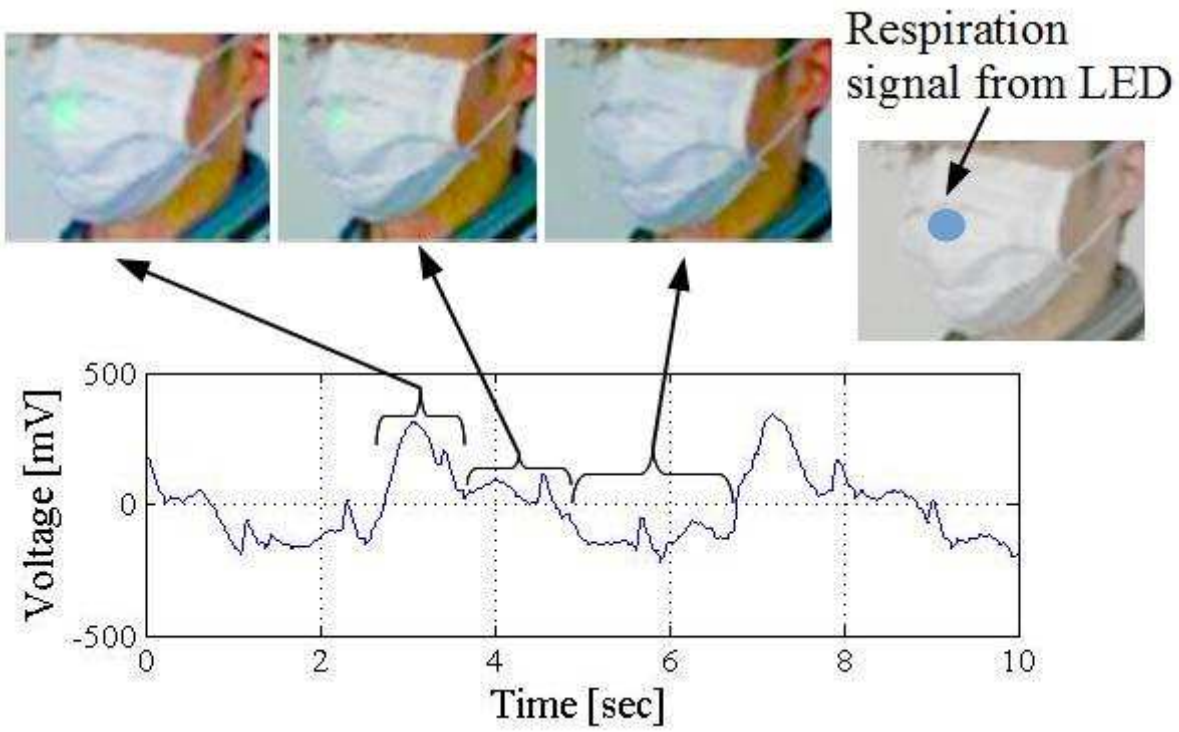

Fig. 18. Compact, low power consumption mask type triage sensor device.

2.5 CONCLUSION

In this paper, we clarified the multiple-input/multiple-output characteristics of piezo devices. The reversibility of the device was explained by the fact that the device has internal feedback. From the analysis of the feedback system, we demonstrated a variety of input and output relations for the device, including the relation between temperature and voltage. Using the characteristics we clarified, we presented a new application for triage. This device which detects and shows the heartbeat and respiration condition of a patient, is set in a mask The signal level of the heartbeat measured by the device was low with a 39.2[dB] S/N ratio, but the signal was accurate enough for use in a triage sensor. The respiration signal level was high with a 55.6[dB] S/N ratio. Using the piezo effect and the pyroelectric effect of the piezo device in the buzzer, we presented a simple, robust, low power, inexpensive, and disposable respiration sensor.

The theoretically calculated impedance in Fig.4 (a) and the experimentally obtained impedance in Fig.4 (b) agreed well in the bands around the anti-resonance and resonance frequencies. However, in the low-frequency range, the experimental impedance was greater than in the theoretical range. We could find no reason for this finding and expect our future work to be able to explain it. Our future work is expected in order to explain this aspect.

REFERENCES

[1] A. J. Fleming, S. O. R. Moheimani, and S. Behrens, ”Synthesis and Implementation of Sensor-Less Active Shunt Controllers for Electromagnetically Actuated Systems,” *IEEE Trans. on Control Systems Technology*, vol. 13, no. 2, pp. 246-261, 2005.

[2] W. Chagjiang, T. Guojun, and W. Nanyan, ”High Performance Speed-Sensor-Less AC Drive System for Induction Motor,” *IEEE TENCON*
’93/Beijng, pp. 602-606, 1993.

[3] M. Norhisam, H. Ezril, M. Senan, N. Mariun, H. Wakiwaka, and M. Nirei, ”Positioning System for Sensor-less Linear DC Motor,” *PECON 2006*, Putrajaya, Malaysia, pp. 476-481, Nov. 28-29, 2006.

[4] Y. Sayouti, A. Abbou, M. Akherraz, and H. Mshoudi, ”Sensorless Low Speed Control With ANN MRAS For Direct Torque Controlled Induction Motor Drive,” *Proceedings of the 2011 International Conference on Power Engineering, Energy and Electrical Drives*, Torremolinos (Malaga), Spain, May 2011.

[5] C. K. Pang, G. Guo, B. M. Chen, and T. H. Lee, ”Self-Sensing Actuation for Nanopositioning and Active-Mode Damping in Dual-Stage HDDs,” *IEEE/ASME Trans. on Mechatronics*, vol. 11, no. 3, pp.328-338, 2006.

[6] A. S. Putra, .S. Huang, K. K. Tan, S. K. Panda, and T. H. Lee,”Self-Sensing Actuation With Adaptive Control in Applications with Switching Trajectory,” *IEEE/ASME Trans. on Mechatronics*, vol. 13, no. 1, pp. 104-111, 2008.

[7] T. Das and R. Mukherjee, ”Shared-Sensing and Control Using Reversible Transducers,” *IEEE Trans. on Control Systems Technology*, vol.17, no. 1, pp.242-248, 2009.

[8] A. Badel, J. Qiu, and T. Nakano, ”Self-Sensing Force Control of a Piezoelectric Actuator,” *IEEE Trans. on Ultrasonics, Ferroelectrics, and Frequency Control*, vol. 55, no. 12, pp.2571-2581, 2008.

[9] M. Rakotondrabe, I. A. Ivan, S. Khadraoui, P. Lutz, and N. Chaillet, ”Simultaneous Displacement/Force Self-Sensing in Piezoelectric Actuators and Applications to Robust Control,” *IEEE/ASME Trans. on Mechatronics*, vol. 20, no. 2, pp.519-531,2015.

[10] Stephen A. Dyer, “Survey of Instrumentation and Measurement,” *Wiley-Inter-science John Wiley & Sons, Inc.*, 2001.

[11] B. Jeffe, W.R. Cook and H. Jeffe, “Piezoceramics,” *Academic*, New York ,1971 .

[12] A. Garner, A. Lee, K. Harrison, and C.H. Schultz, “Comparative analysis of multiple incident triage algorithm,” *Annals of emergency medicine*, vol.38, no.5, pp.541-548, 2001.

[13] M Asadnia, A G P Kottapalli, J M Miao1, A B Randles, A Sabbagh, P Kropelnicki and J M Tsai, “High temperature characterization of PZT(0.52/0.48) thin-film pressure sensors,” *J. Micromechanics and microengineering*, vol.24, no.1 pp.1-12., 2013.

3.Respirometer by a piezo device and its application to triage

Abstract: In this paper, we present a novel respirometer using the effect of piezo devices and show its application to triage. We found that blowing on the piezo device generated several hundred millivolt voltage and also it synchronizes with the respiration. Our detail investigations on the phenomena showed that it was caused by the pyroelectric effect. In general, the piezo device when used as a sensing device generates output voltage in a battery-less manner and also functions as a buzzer, which can lead to a compact, simple and low-power respirometer. Here the piezo device was used as a base of respirometer, and used not only as a respirometer but also as an alarm sound generator. Thus the proposed respirometer was realized only by one piezo device and a low-powered microprocessor driven by a small battery. We applied the respirometer to triage and realized a triage sensing system. In the system, we employed the triage priority determination procedure defined as an international standard. The triage sensing system set in a mask detects respiration and displays its condition by turning an LED on and off synchronizing the respiration and also generates the alarm sound when the respiration falls into the pre-specified ill-conditions.

Keywords: respirometer, piezo device, pyroelectric, triage

3.1 INTRODUCTION

A class of devices exhibit reversible characteristics. These devices function not only as actuators but also as sensors. One example of the applications using the reverse functions is a sensor-less time-sharing automatic feedback control [1]-[9]. In this paper, we focused on a piezo device which has reversible characteristics and the reversibility is explained by the existence of an internal feedback in the device [10].

The piezo devices are applied in a variety of fields as electronic filters, electronic oscillators, sound generators, acceleration and vibration sensors and vibrators, igniters, etc., [11]. Among these applications, the most common use of the devices are as electronic filters; hence, the piezo devices have been modelled by an equivalent electrical circuit [11] in spite of the fact that electrical, mechanical, and thermal phenomena occur and interact with each other through a feedback loop in the device. The equivalent electrical circuit model shows only one aspect of the phenomena occurring in the device, and thereby, limits the true potential of the device.

In this paper, we focus on the thermal–electrical pyroelectric effect which induces voltage when the device is heated. Based on the effect, we proposed a compact, simple and low-powered respirometer which can be set in a mask and displays the respiration conditions optically by turning an LED on and off in synchronizing with respiration and also generates alarm sound when the respiration falls into the ill-conditions by using the device itself.

3.2 CHARACTERISTICS OF PIEZO DEVICE

A. Model of pyroelectric effect of piezo device

Figure 1 shows a piezo device used in buzzers.

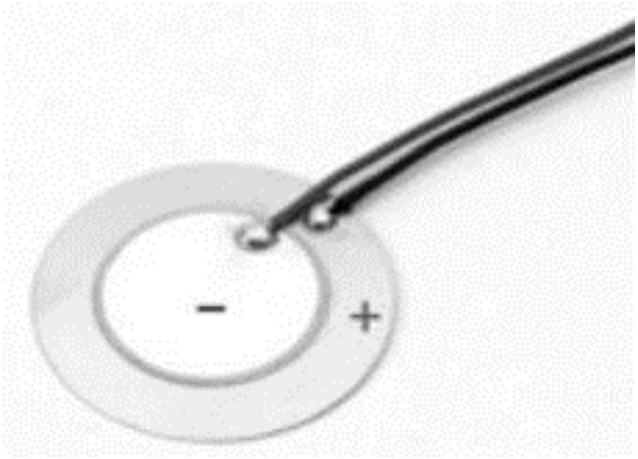

Fig. 1. Piezo device used in buzzers and will be used in the proposed respirometer

Define the constants and variables of the piezo device as follows;

<General variable>

t: time

<Electrical constants>

d: gap between electrode plates

Q: permanent electric charge in piezo material because of residual polarization

C: capacitance

<Thermal constants>

K: pyroelectric constant of piezo material

T_c: thermal time constant

<Mechanical constants>

m: mass of the movable plate

D: damping coefficient of plate

k: stiffness constant of plate

<Electrical variables>

$e(t)$: input voltage

$E(t)$: output voltage

$q(t)$: electric charge generated by adding strain or by feeding voltage between electrodes

$i(t)$: electric current given by a time derivative of $q(t)$

$q_T(t)$: total electric charge including pyroelectric effect

< Mechanical variables>

$f(t)$: externally fed force

$F(t)$: total output force because of externally fed force and piezo effect force

$x(t)$: input displacement

$X(t)$: total output displacement

< Thermal variables >

$\Delta T(t)$: temperature difference between front electrode and atmospheric temperatures at the rear electrode

< Biological variable>

$E_r(t)$: respiration signal

Then the reversibility characteristics of the piezo device can be represented by a feedback as shown in the block diagram in Figure 2 [10].

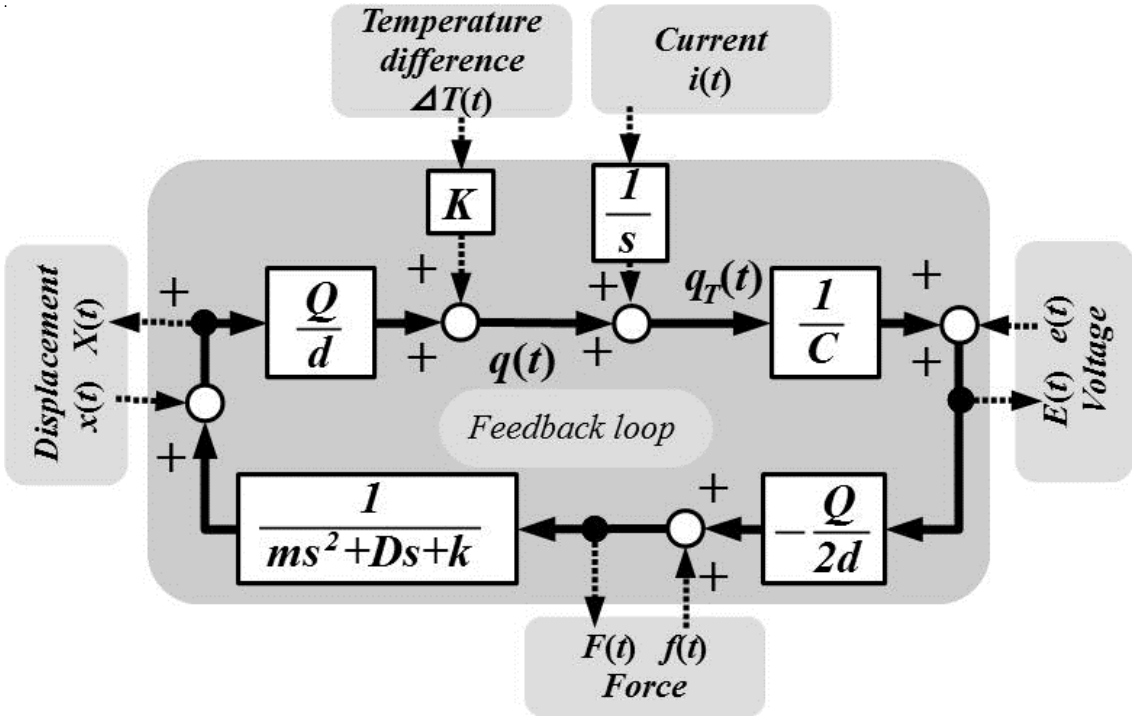

Fig. 2. Block diagram showing the internal feedback signal flows in the piezo device.

From the block diagram in Fig.2, the transfer function of the output voltage $E_r(t)$ with respect to the change in temperature difference $\Delta T(t)$ is given as follow:

(1)

Transfer function in eq. (1) expresses the characteristics of the pyroelectric effect. Immediately after a temperature change, the transfer function can be approximated as follows from eq.(1) using the initial-value theorem of Laplace transform:

(2)

B. Output voltage by the pyroelectric effect

In order to show that the piezo device generates voltage by heating its surface, we carried out the experiments. Figure 3 shows the experimental setup. A blower, which blows air at different temperatures, was set in one of the devices. Note that the peak air-flow speed in normal human exhalation is around 0.5m/s and the temperature is around 36℃, which are the conditions cited in our examinations. The 26℃ room-temperature airflow at speeds ranging from 0.5m/s to 10.0m/s, and the 36℃ airflow at a speed of 0.5m/s, were fed to the device. Figure 4(a) shows the output voltage when the 26℃ room temperature airflow at a speed of 10m/s was fed. The output DC voltage is steady at approximately 0V, and its amplitude is 8.6mV. When air-flow at the same room temperature and 5.0m/s speed was fed, the output DC voltage was again steady and the amplitude was 4.2mV. Similarly, when airflow with 0.5m/s speed was fed, the amplitude was 3.0mV. On the other hand, Fig. 4(b) shows the output voltage when airflow at 36℃and 0.5m/s speed (human exhalation) was fed. The output voltage suddenly increased to 743mV and gradually attenuated to 0V.

These results show that output voltage change occurred not by the dynamic pressure applied to the piezo device but by the temperature change in the device, which was caused by the pyroelectric effect.

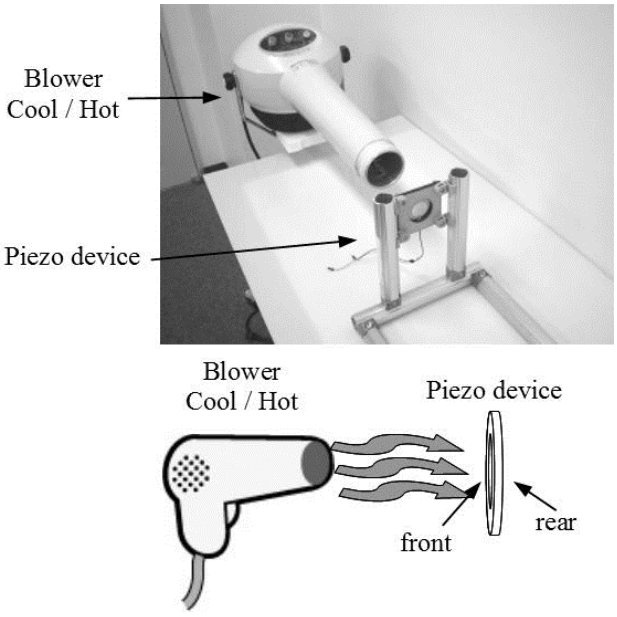

Fig.3 Experimental setup to investigate the effect of dynamic pressure by airflow and pyroelectric effect

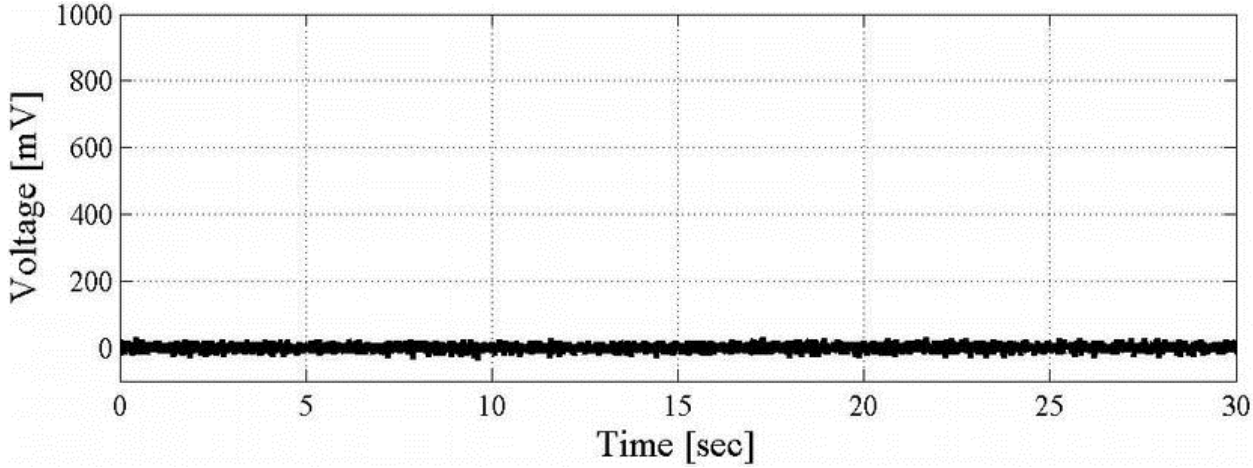

(a) Output voltages for airflow at 26℃and 10.0m/s

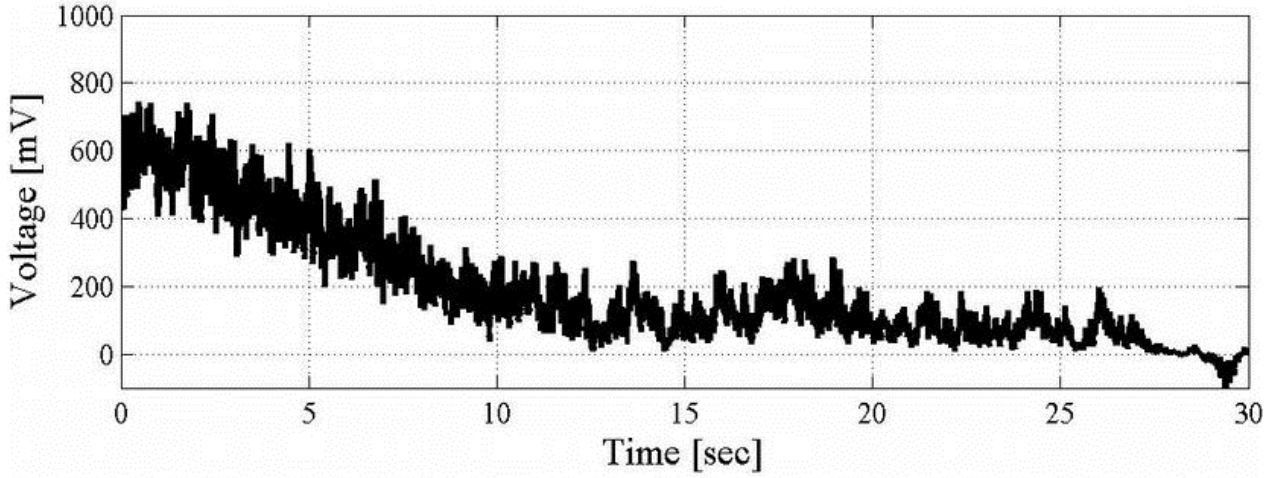

(b) Output voltages for airflow at 36℃and 0.5m/s

Fig.4 Output voltages when blowing on room-temperature and hot (human body) temperature airflows

From Fig.4 (a), when the circumference temperature is same with the blowing temperature, zero output voltage comes out. We investigated the relation between the circumference temperatures and the blowing temperature. Figure 5 shows the circumference temperature vs. output voltage under the constant blowing temperature of 36.4℃.

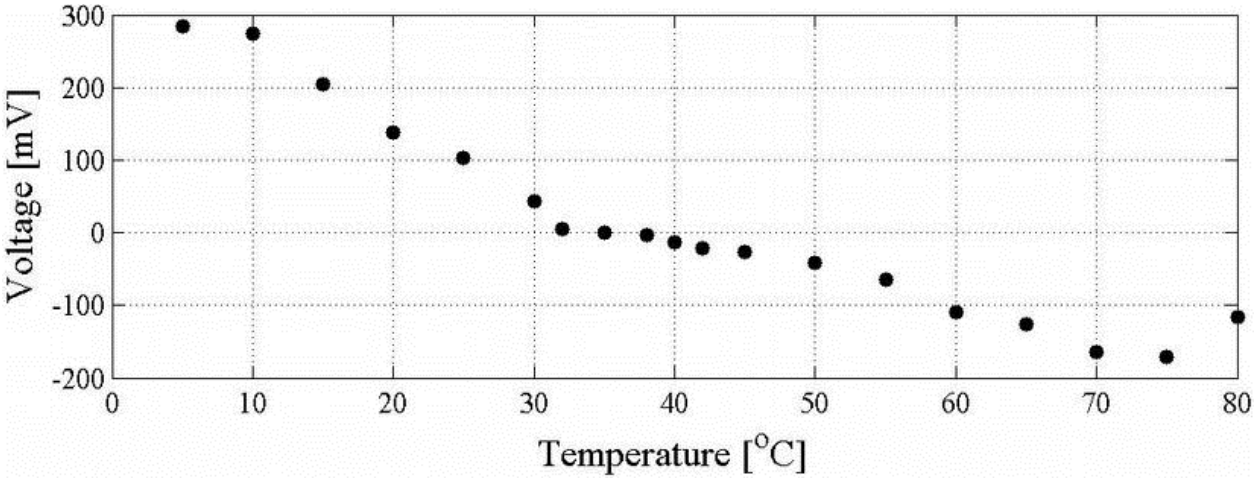

Fig.5 Circumference temperature vs. output voltage

Fig.5 shows that when the circumference temperature is near to the blowing temperature, the output voltage is zero, when the circumference temperature is lower than the blowing circumference, the output is positive, and when the circumference temperature is higher, the output voltage is negative. Slight difference between the circumference and blowing temperatures generates the non-zero output voltage.

3.3 RESPIROMETER USED IN TRIAGE

Among a variety of applications of respirometers, here, we focus on triage. Serious natural disasters such as a major earthquake, or tsunami, or man-made disasters such as suicide bombing by terrorists leave many injured at once, and the hospitals may not be able to provide sufficient medical care. After the Great East Japan Earthquake, the wounded lay on beds, couches, and even on the floor, in dark passages. Their conditions changed with the time and some died from the lack of sufficient attention and cares from medical staffs. Triage is a priority determination procedure of cares, which ensures proper assignment of the available care resources in the most effective manner. It also helps in classifying the patients as: 0: DEAD (black card), I: IMMEDIATE (red card), II: DELAYED (yellow card), and III: MINOR (green card). The patients are cared for in order, from I to III. The simple triage and rapid treatment (referred to as START) is one of the international standard methods. The priority is determined based on the flow chart in Figure 6 [12]. In this process, the bio-signals employed are: (1) visual inspection of ambulatory ability, and (2) respiration.

Therefore, if respiration can be detected automatically, it would be extremely useful for triage.

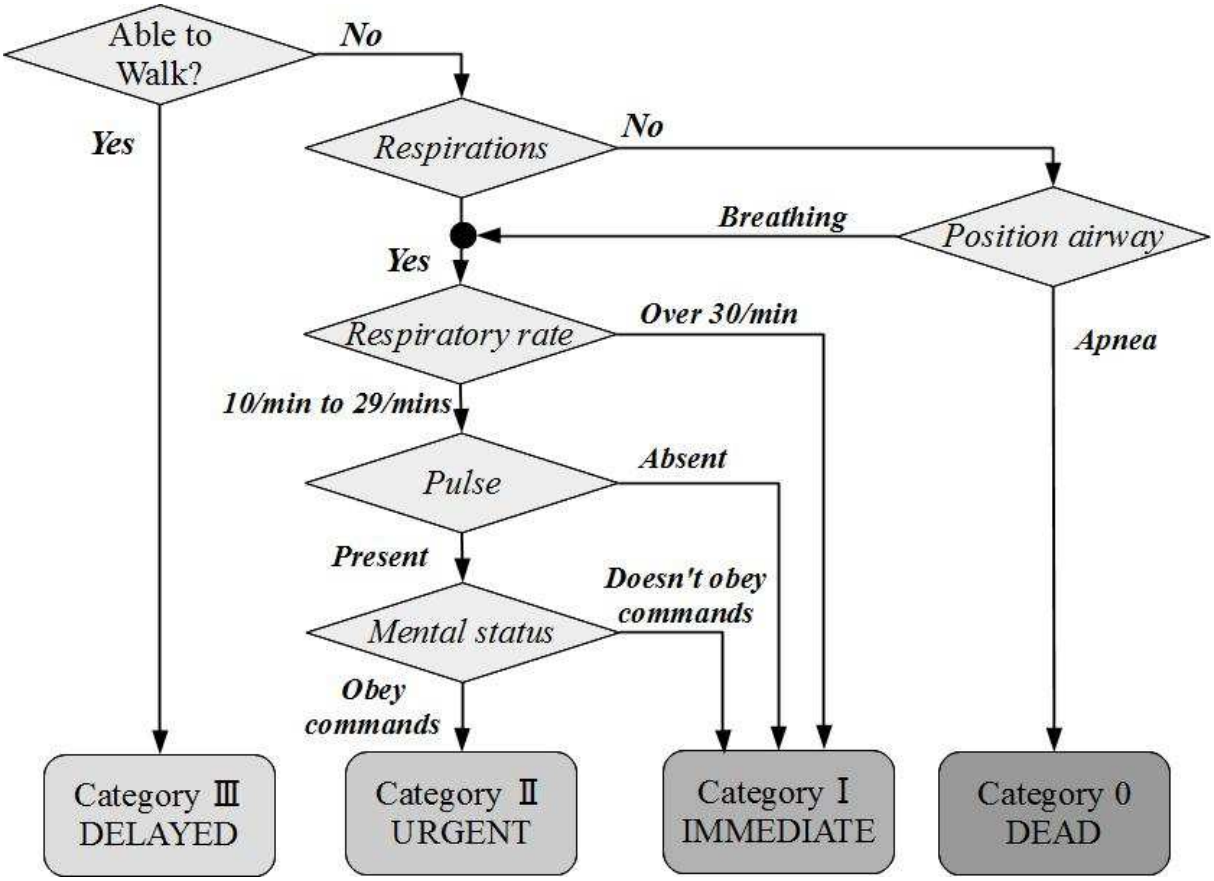

Fig. 6. The simple triage and rapid treatment (START) process

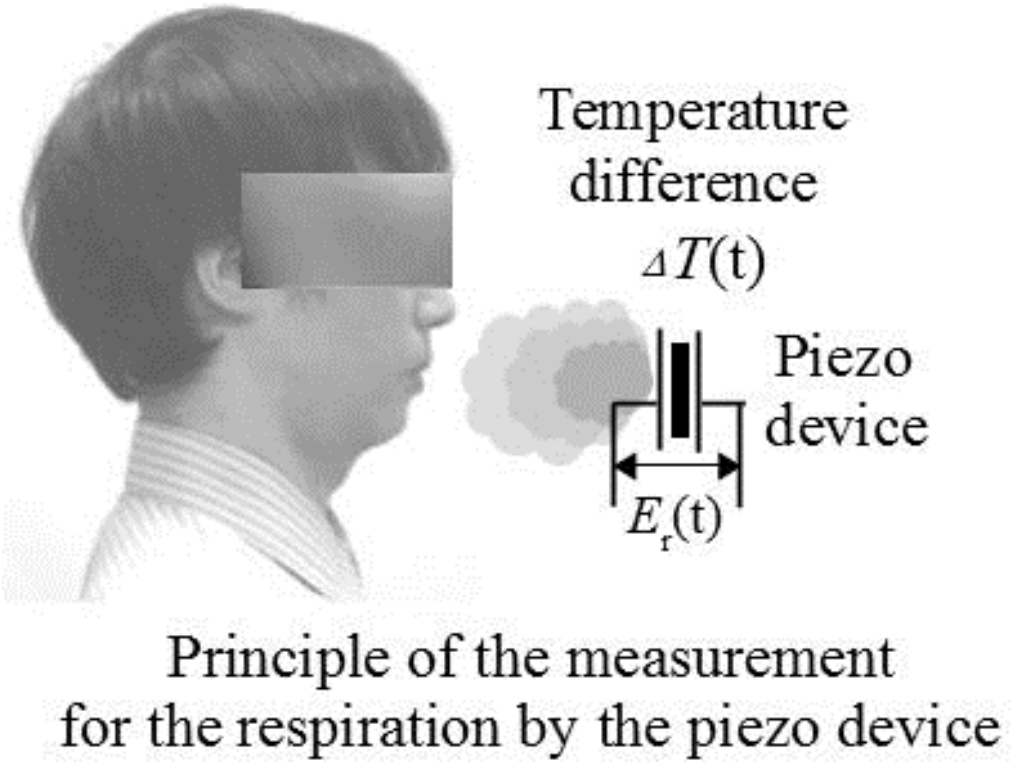

Fig. 7. Measurement principles of respiration using a piezo device

Figure 7 shows the measurement principles used to detect the respiration using a piezo device. The exhaled hot air arrives at the surface of the piezo device when the patient breathes, and a temperature difference $\Delta T(t)$ occurs between the mouth side and other side of the device. Then the device generates a voltage $E_r(t)$ in accordance with the transfer function eq.(1) of voltage with respect to temperature.

3.4 EXPERIMENTAL VERIFICATIONS

The experimental data were acquired following to the informed consent procedure described in the human associated researches rule (1141) enacted by Hosei University [13].

A. Experimental setup

Figure 8 shows a proposed mask-type respirometer for triage based on the principle shown in Fig. 6. The piezo device is set at the top of a mask, and the piezo material is inside the mask such that the exhaled hot air arrives directly at the piezo device.

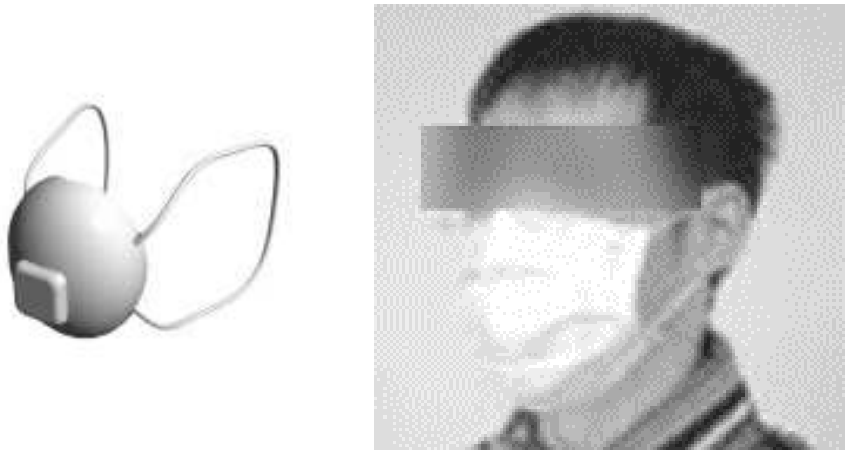

Fig. 8. Proposed respirometer for triage

Figure 9 shows the experimental setup using the proposed system. We also measured the respiration signals using a microphone-type respirometer for comparison.

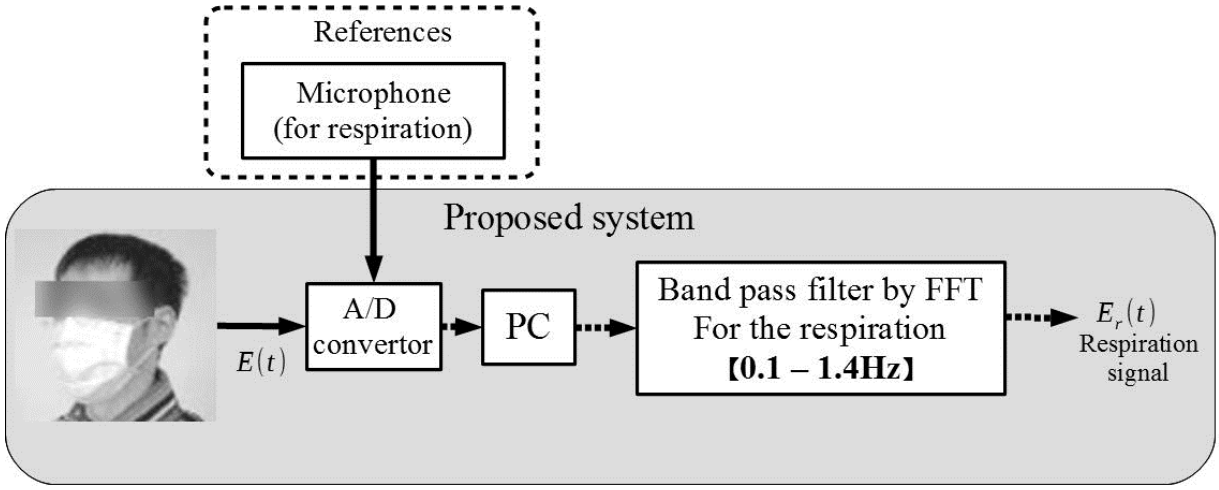

Fig. 9 Experimental setup and conditions for measuring respiration using the system in Fig.7

The output from the piezo device was directly AD converted without using an amplifier, and transferred into a personal computer (OPTIPLEX 960). The voltage range of the AD converter (NR-2000) was set as ±1.0V and the sampling interval was set to 1.0ms. The signal acquired was digitally filtered using a non-recursive FFT method. A bandpass filter with a pass-band from 0.1Hz to 1.4Hz was employed to acquire the respiration signal.

B. Experimental results

Figure 10 shows the respiration signal $E_r(t)$. The slow-changing wave with the positive peak voltage of 500mV and the negative peak voltage of -200mV is the respiration signal from the piezo device and the fast-changing wave with the amplitude of 100mV is that from the microphone-type respirometer. They synchronize each other. The S/N ratio for the measurement by the proposed piezo device was 55.6dB. The output voltage of respiration is high and even a weak respiration can be detected.

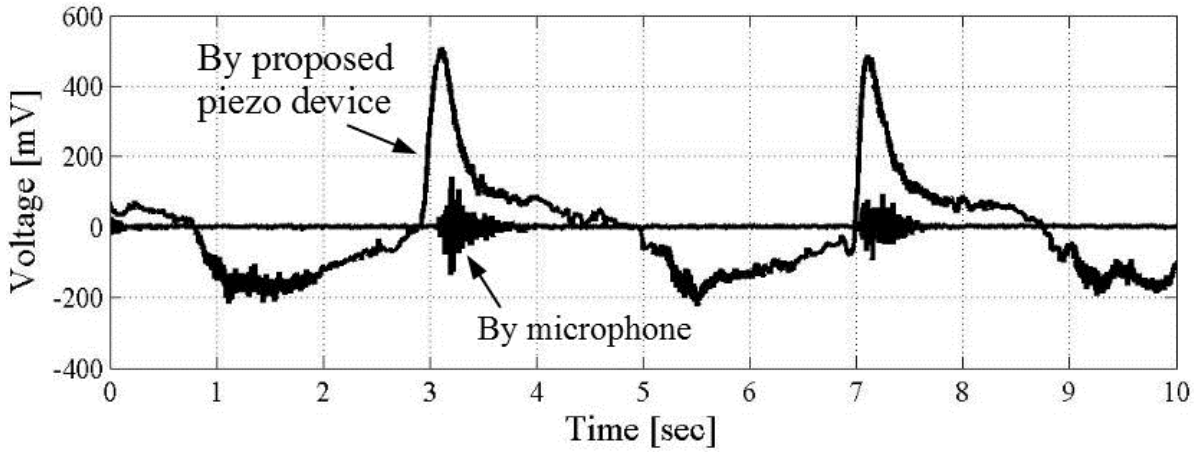

Fig. 10 Non-recursive digital bandpass filtered respiration signal $E_r(t)$ detected by the piezo device, and the respiration signal measured by the microphone-type respirometer. The band was from 0.1Hz to 1.4Hz. The S/N ratio was 55.6dB

3.5 TRIAGE SENSOR

Figure 11 shows a device for triage sensor realized by using PIC16LF1554-1/SL-ND microprocessor. The triage priority determination procedure is followed to the flow chart shown in Fig.5 and working procedures are as follows:

(1) Waiting (mask setting) time is 10s and 10s after switch on, the device begins to measure respiration.

(2) If the respiration is ceased for 30s the buzzer generates continuous 2kHz sound.

(3) If respiation frequency is less than 9 per minute, the discreate 2kHz sound of every 1s with duty ratio 0.9 is generated.

(4) If respiation frequency is greater than 30 per minute, the discreate 2kHz sound of every 0.5s with duty ratio 0.8 is generated.

When the piezo device and the preamplifier have the high insulation impedance, the electric charge generated by the pyroelectric effect hardly discharges from the device. This yields the situation that the device and the preamplifier functions as the peak hold circuit, where once the peak voltage is holed, the voltage lower than the peak does not occur. To avoid this phenomena, we let the microprocessor reset and dischage the charge every time just after the respiration voltage is measured.

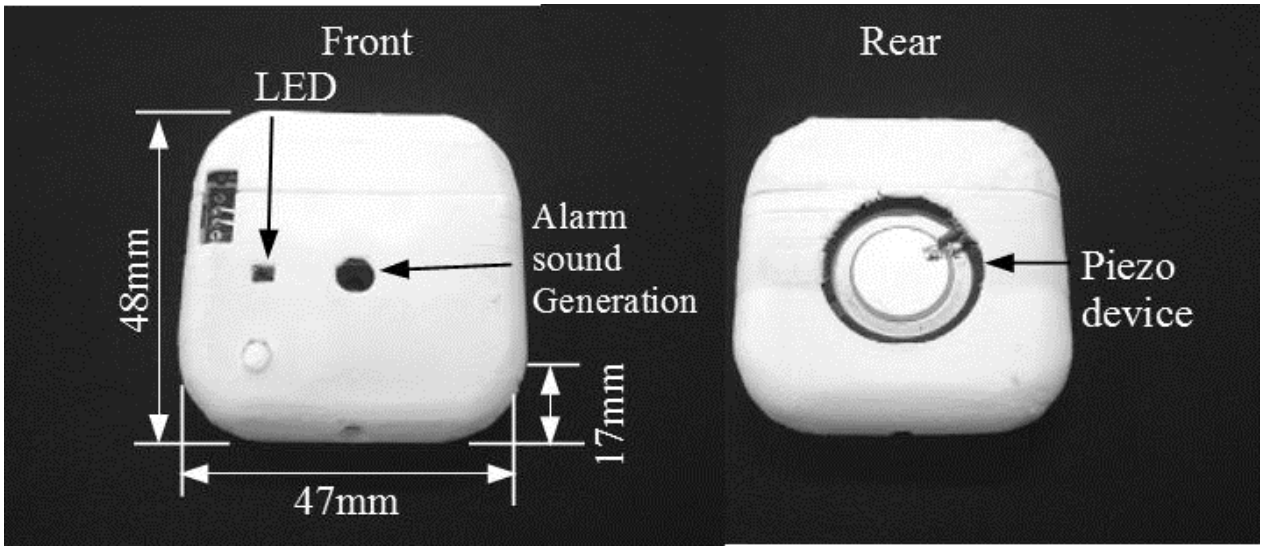

Fig.11 Developed triage sensor

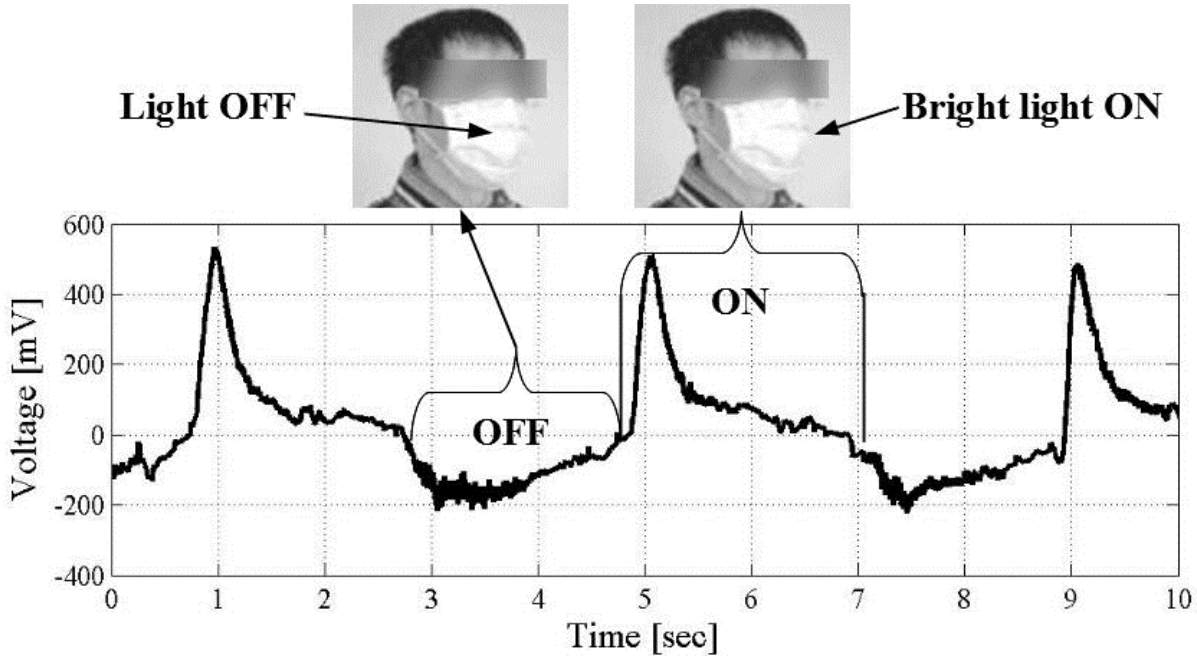

Fig.12 LED emission in synchronizing with the respiration

Figure 12 shows the LED lighting in synchronizing with the respiration.

Experiments under 10 time trials by 25 healthy subjects using the sensor in Fig.10 showed 100% correct judgments of respiration status defined by the international triage diagnosis and/or decision procedures.

3.6 ***CONSIDERATIONS***

Fig.4(b) shows that the output voltage suddenly increased after the step change in temperature and gradually attenuated to 0V. This phenomenon is explained by the theoretical results given by the transfer function in eq. (1) of the output voltage with respect to the change in temperature difference. The transfer function includes the high-pass filter characteristics $sT_c/(1+sT_c)$ with the time constant T_c, which cuts off the DC component and the output voltage decreases to zero with the time constant T_c. From Fig.4(b) the time constant T_c is about 12s which is long enough not to filter out the voltage by respiration.

Putting on a less air permeable mask may let patients feel stuffy. This can be one demerit of the proposed method. The piezo device on the other hand can work even when it is set on a mask of single piece of gauze with good air permeability. This type of mask may release the stuffy feeling. Furthermore the device can detect the normal respiration blowing 20cm apart from the mouth. Some noninvasive setting of device other than the mask basing on the characteristics above provides less stuffy feeling.

3.7 CONCLUSIONS

In this paper, we presented a novel respirometer which uses the pyroelectric effect of piezo devices and shows an application for triage. The device set in a mask can detect respiration with a 55.6dB S/N ratio. Using the piezo effect and the pyroelectric effect of the piezo device in the buzzer and a signal processor, we presented a compact, simple and low power sensor. Experiments under 10 time trials by 25 healthy subjects using the sensor 100% correctly judged the respiration conditions defined international triage priority determination procedures.

REFERENCES

1. A. J. Fleming, S. O. R. Moheimani, and S. Behrens, (2005) Synthesis and Implementation of Sensor-Less Active Shunt Controllers for Electromagnetically Actuated Systems, IEEE Trans. on Control Systems Technology, 13-2:246-261
2. W. Chagjiang, T. Guojun and W. Nanyan (1993) High Performance Speed-Sensor-Less AC Drive System for Induction Motor, IEEE TENCON'93/Beijng: 602-606
3. M. Norhisam, H. Ezril, M. Senan, N. Mariun, H. Wakiwaka, and M. Nirei (2006) Positioning System for Sensor less Linear DC Motor, First International Power and Energy Conference PECON November 28-29, Putrajaya, Malaysia : 476-481
4. Y. Sayouti, A. Abbou, M. Akherraz, and H. Mshoudi (2011) Sensorless Low Speed Control With ANN MRAS For Direct Torque Controlled Induction Motor Drive, Proceedings of the 2011 International Conference on Power Engineering, Energy and Electrical Drives, Torremolinos (Malaga), Spain, May
5. C. K. Pang, G. Guo, B. M. Chen, and T. H. Lee (2006) Self-Sensing Actuation for Nanopositioning and Active-Mode Damping in Dual-Stage HDDs," IEEE/ASME Trans. on Mechatronics, 11-3,:328-338
6. A. S. Putra, .S. Huang, K. K. Tan, S. K. Panda, and T. H. Lee (2008) SelfSensing Actuation With Adaptive Control in Applications with Switching Trajectory IEEE/ASME Trans. on Mechatronics, 13-1: 104111
7. T. Das and R. Mukherjee (2009) Shared-Sensing and Control Using Reversible Transducers IEEE Trans. on Control Systems Technology 17-1:.242-248
8. A. Badel, J. Qiu, and T. Nakano (2008) Self-Sensing Force Control of a Piezoelectric Actuator IEEE Trans. on Ultrasonics, Ferroelectrics, and Frequency Control 55-12:2571-2581
9. M. Rakotondrabe, I. A. Ivan, S. Khadraoui, P. Lutz, and N. Chaillet (2015) Simultaneous Displacement /Force Self-Sensing in Piezoelectric Actuators and Applications to Robust Control IEEE/ASME Trans. on Mechatronics 20-2:519-531
10. T. Yoshida, K. Kobayashi, Y. Kurihara, N. Shiroi, and K. Watanabe (2017) Multiple-Input/Multiple-Output Characteristics of Piezo Devices and an Application for Triage IEEE SENSORS JOURNAL 17-5:1434-1442
11. B. Jeffe, W. R. Cook, and H. Jeffe (1971) Piezo ceramics. New York, NY, USA: Academic,
12. Alan Garner, Anna Lee, Ken Harrison, and Carl H Schultz (2001) Comparative analysis of multiple-casualty incident triage algorithms. Annals of emergency medicine 38-5: 541-548
13. Hosei University (revised 2016) Ethical rule for the human associated researches Rule book of Hosei university, Rule 1141

4.Powder and Bulk Level Monitoring by an Acoustic Tube Method

Abstract— This paper describes a novel acoustic-tube level switch that detects hot powder and finely gained bulk. The tube length L is selected as $L=n\times(\textit{half-wavelength})$ and the input port of the tube is acoustically driven by a piezo-sounder. When the output detection port is covered by powder and bulk, the electric impedance of the sounder increases with the increase of the acoustic impedance of the tube. The wavelength of a constant frequency increases proportionally to the temperature, which causes a deviation from the optimal length L above. However, theoretical studies showed that covering the detection port mostly influences the acoustic viscosity and robust to the temperature. As a result, the method worked well in a wide temperature range. The method operated consistently in the range ±50°C from the reference and detected powder and bulk with 13 kg/m^3 bulk density. Additionally, the technique reliably detected level of gravel heated to 450°C; in this case, the tube functioned as a heat radiator. Furthermore, the sound at the detection port could blow out dust accumulated in the tube. A dust filter located at the quarter-wavelength position had little influenced on the normal measurement function, even for a dust layer of 26.5 mm thickness.

Index Terms— powder and bulk, level switch, acoustic tube, low-bulk-density, high-temperature.

4.1 INTRODUCTION

Level meters are industrial instruments that detect the surface level between a gas and a liquid, between different liquids, or between a gas or liquid and powder and bulk. The level meters can be categorized as continuous type, which measures the surface continuously, and level switch, which evaluates whether the surface reaches a specified level. Despite the difficulty of the associated measurement technique, continuous-type level meters are mainly used for simple monitoring of a level, whereas level switches, which seem to involve an easy technique, are used as sensors for condition-sequence control purposes [1]. Thus, level switches require high reliability and stability. A liquid-level meter is relatively easy to realize owing to the continuity characteristics of liquids. For example, the most popular continuous differential pressure level meters measure the pressure difference p between the bottom and the top of a liquid. When the density of the liquid is ρ and the liquid level is h under gravity g, the pressure difference p is given by $p=\rho gh$; thus, the level of the liquid is obtained from the measured pressure as $h=p/\rho g$.

Continuous liquid-level meters include those using microwaves [2]–[5], those using ultrasonic [6] and a method that assesses the level by the tone of the tank hitting sound [7], and a technique that employs the optical reflection of a thin core fiber installed in a liquid tank and a noncontact capacitance-type level transducer [8]. In contrast to the liquid level meter, few new researches of the powder and bulk point level meters are available [9,10], which use the microwave radar technique. The old and simple methods such as the diagram switch, paddle level switch, tilet level switch, capacitive level and vibrating level switch are major in powder and bulk plants. This is because powders and bulk solids behave in a complicated manner [11] which cannot be described the physical laws to explain the behaviors. Furthermore bulks stored in a tank cover a very large variety of substances like grains, powder, sand, plastic pellets, ash and also very rough materials like stones, coal, and others [11]. Additionally, the temperature of the bulks can vary widely, ranging from room

temperature to several hundred degrees centigrade, in the case such as combustion ash and dust adhesion to the instrument always occurs. Thus, in the powder and bulk level measurement, a variety of measurement principles have been employed.

Among above old and simple methods, the vibrating level switch by a tuning fork is widely used and is ideal for use either in adhesive and abrasive substances as well as bulk solids with very low density. However the tuning fork faces heavy stress when it is covered and suppressed by powder and bulk and the folk is frequently bent and destroyed. To avoid such the situation, instead of using mechanical vibration, we considered to use acoustical vibration where there is not any mechanical vibrating component. Authors previously proposed an acoustic level switch for bulks and powders [12,13] which detects the change in the impedance of an acoustic tube when the detecting port is covered by the powder and bulk. In the previous works, we developed a theoretical model and showed the feasibility via simulations [12] and simple laboratory experiments [13]. Here we newly investigate the feasibility of the acoustic method, under realistic conditions that a large environmental temperature changes occurred and also the temperature of powder and bulk was high.

4.2 ACOUSTIC TUBE LEVEL SWITCH

A. Proposed level switch

Figure 1 shows the proposed acoustic-tube level switch. Consider a storage tank ① with a port in which an acoustic tube with uniform cross sectional area ② is inserted. The tube is acoustically excited by a piezo-sounder ③ at its resonance frequency. The detection port of the tube is inside the tank. When the detection port is covered by powder and bulks, the acoustic impedance of the tube is modified, leading to the change in the electric impedance of the piezo-sounder. This change is detected by a divider electric circuit ④, and the voltage is acquired by a processor ⑤ to evaluate switching using dynamic-threshold logic. The length of the acoustic tube is $n\times$(*half-wavelength*), where n is an integer number and the wavelength is determined by the resonance frequency of the sounder and the average temperature around the tank. When the length is $n\times$(*half-wavelength*), a dust filter ⑥ is placed at the position $(2n+1)\times$(*quarter-wavelength*), where the filter has less influence on acoustic phenomena. The filter setting position of the tube is easily dis-connectable and attachable for easy filter changing. The motion energy of air at the detection port can blow out dust accumulated in the tube.

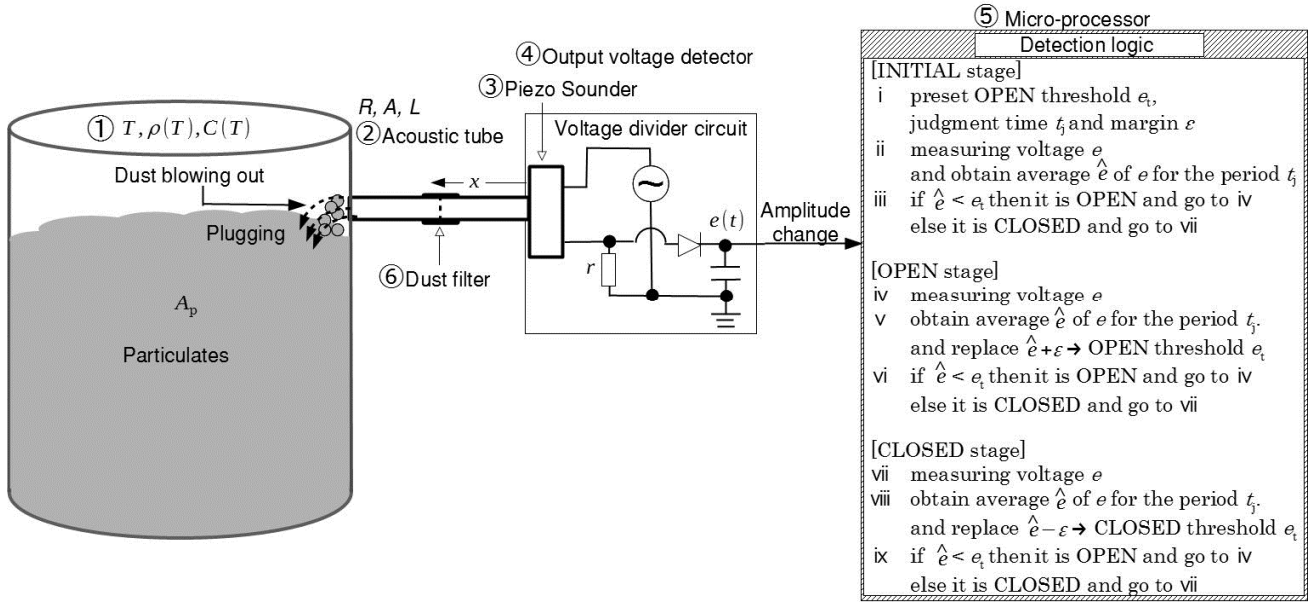

Fig.1 Proposed acoustic-tube level switch for particulates

This level switch focuses on the detection of light and hot powders or fibers and is used in the following conditions.

(C1) The temperature difference at the acoustic input port outside the tank and the detection output port inside the tank is approximately 100°C and the temperature is distributed linearly along the acoustic tube. Furthermore, the environmental temperature changes ±50℃ with respect to the reference temperature.

(C2) The powders or fibers in the tank have low bulk density and the air can pass through them without acoustic reflection. Thus, the acoustic characteristics are viscous and the air-passing area is slightly smaller than the cross sectional area of the acoustic tube.

Hot combustion ash is an example of powders under condition (C1). The temperature of the combustion ash in the tank is several hundred degrees centigrade, and the part of the metal acoustic tube that is located outside the tank radiates heat and decreases the temperature. If the temperature remains high, equipping the tube with a radiation fin considerably decreases the temperature. From the various temperature distribution profiles along the tube, we selected the typical but simple linear distribution profile. The change of the environmental temperature in the range $\pm 50℃$ is also a strict condition. The viscosity that satisfies condition (C2) is given by (air density)×(sound velocity)/(area through which air can pass). For example, for the air in a cylindrical tube with diameter 1.0cm, the viscosity is 12.4×10^5 Pa/(m^3/s) or 12.4 acoustic ohm. Under the conditions described above, the acoustic-tube level switch suffers from environmental disturbances, namely, the change in the environmental temperature and the dust that may be accumulated in the tube. The proposed method handles these disturbances using various strategies: the temperature robustness of the method itself, a dust blow-out function, a dust-filtering function, and ultimately, if these fail, using the dynamic threshold approach for switching judgment. The proposed method has a very simple structure. In the study, we theoretically investigated the temperature robustness and experimentally verified the robustness, dust blowing and filtering functions, as well as the validity of the dynamic threshold strategy.

B. Variables and constants

The employed variables and constants are defined as follows:

ω: sound angular frequency [rad/s]

f: sound frequency ($=\omega/2\pi$) [Hz]

<Environment and powders>

P: atmospheric pressure [atm]

$T(x)$: air temperature at location x [°C]

T_o: environmental temperature [°C]

T_H: temperature at detection port [°C]

τ: temperature deviation from T_o [°C]

$\rho(T)$: air density [kg/m^3]

$C(T)$: sound velocity [m/s]

$\lambda(T)$: sound wavelength [m]

$\theta(\tau)$: angle [rad]

A_p: area of the powders through which air can pass, which is inversely proportional to the bulk density of the powders [m^2]

R_a: viscous resistance of the powders [Pa/(m^3/s)]

d_a: mechanical viscous coefficient [N/(m/s)]

<Piezo-sounder>

m: total mass of sounder and air in the cavity [kg]

k: total spring constant of sounder and air in the cavity [N/m]

D: mechanical damper coefficient [N/(m/s)]

d: gap between electrodes or thickness of piezo-device [m]

C: capacitance of the piezo-device [F]

Q: permanent charge in the piezo-device [C]

$Z_e(i\omega)$: electric impedance of the sounder at ω [Ω]

f_r: resonance frequency of sounder with acoustic tube [Hz]

f_{ar}: anti-resonance frequency of sounder with acoustic tube [Hz]

ζ : damping coefficient [-]

<Acoustic tube>

A: cross-sectional area of the acoustic tube ($=\pi R^2$) [m^2]

L: length of the acoustic tube [m]

$Z_a(i\omega)$: acoustic impedance at ω [Pa/(m^3/s)]

<Divider circuit>

r: divider resistance for output [Ω]

$e(t)$: output voltage [V]

<Detection logic>

e_t: threshold voltage [V]

t_j: judgment time [s]

ε: margin of threshold [V]

C. Acoustic impedance and mechanical spring constant

The air density $\rho(T)$, sound velocity $C(T)$, and angle $\theta(\tau)$ are given as follows:

$$\rho(T)=\frac{1.239\times P}{1+T/273.15} \qquad (1)\ [(A3)]$$

$$C(T)=331.5\text{m/s}+0.6T \qquad (2)\ [(A4)]$$

$$\theta(\tau)=\frac{\omega L}{0.6(T_{\mathrm{H}}-T_{\mathrm{o}})}\ln\left|1+\frac{0.6(T_{\mathrm{H}}-T_{\mathrm{o}})}{C(T_{\mathrm{o}})+0.6\tau}\right| \qquad (3)\ [(A15)]$$

From the previous theoretical investigation [13], the acoustic spring constant is given by a complex number for a tube with arbitrary length L under conditions (C1) and (C2) as follows:

$$\mathrm{i}\,\omega A^2 Z_{\mathrm{a}}(\mathrm{i}\omega)=\omega\frac{\rho(T_H)C(T_H)}{A_{\mathrm{p}}}A^2\frac{1+tan^2\theta(\tau)}{1+\left(\frac{A}{A_{\mathrm{p}}}\tan\theta(\tau)\right)^2}\left\{\mathrm{i}+\frac{1}{2}\left(\frac{A}{A_p}-\frac{A_p}{A}\right)\sin 2\theta(\tau)\right\} \qquad (4)$$

which is a function of the angle $\theta(\tau)$ or, eventually, a function of the temperature deviation τ from the environmental temperature T_0. The imaginary part of eq.(4) is always positive and indicates the viscosity characteristics, and the real part can be positive or negative according to the sign of $\sin 2\theta(\tau)$. If it is negative, it shows the mass characteristics, and if positive, it reveals the spring characteristics. Figure 2 shows the loci of $\mathrm{i}\,\omega A^2 Z_{\mathrm{a}}(\mathrm{i}\omega)$ when the acoustic angle $\theta(\tau)$ changes from $\frac{\pi}{2}$ (generally $\frac{2n+1}{2}\pi$) to π (generally $n\pi$).

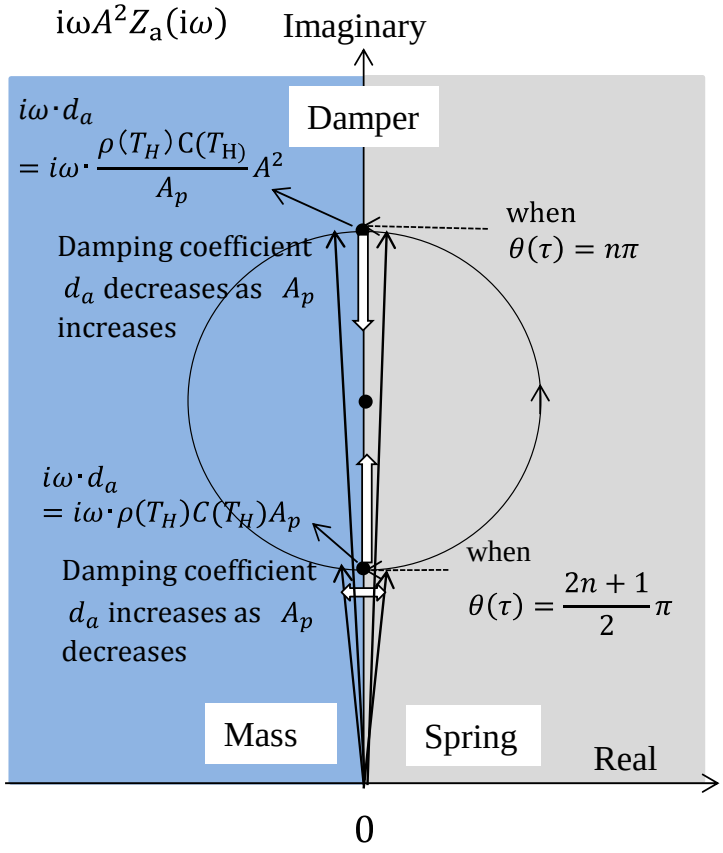

Fig.2 Loci of the mechanical impedance for varying angle $\theta(\tau)$

As shown in Fig.2, from eq.(4), when $\theta(\tau) = n\pi$ (thus, $\tan\theta(\tau) = 0$), $\mathrm{i}\,\omega A^2 Z_\mathrm{a}(\mathrm{i}\omega)$ has only an imaginary part and the real part becomes 0.

$$\mathrm{i}\omega d_\mathrm{a} = \mathrm{i}\omega \frac{\rho(T_0)C(T_0)}{A_\mathrm{p}} A^2 \quad (5)$$

The acoustic tube shows only the viscosity characteristics. Furthermore, when $A_\mathrm{p} = 0$, i.e., the detection port is completely closed, $d_\mathrm{a} = \infty$.

In these situations, the acoustic tube functions as a damper. From condition (C1), $\rho(T_\mathrm{o})C(T_\mathrm{o}) \cong \rho(T)C(T) \cong \rho(T_\mathrm{H})C(T_\mathrm{H})$, and d_a is robust against temperature changes but is substantially influenced by the area A_p, which is inversely proportional to the bulk density of the powders or fibers in the tank.

When the tube length is $L = n \times (half\ wavelength)$,

$$L = \frac{n}{2} \cdot \lambda(T_0) = \frac{nC(T_0)}{2f} = \frac{n\pi C(T_0)}{\omega} \quad (6)$$

and the angle $\theta(\tau)$ is given as follows:

$$\theta(\tau) = n\pi \cdot \frac{C(T_0)}{0.6(T_H - T_0)} \cdot \ln\left|1 + \frac{0.6(T_H - T_0)}{C(T_0) + 0.6\tau}\right| \quad (7)$$

When $T_H = T_0$ and $\tau = 0$, i.e., there is no difference between the environmental temperature and the temperature of the detection port and no temperature deviation, the angle in eq.(7) is $\theta(\tau) = n\pi$, which results in the situation described by eq.(5)

We calculated the complex spring constant of eq.(4) for $T_0 = 50\ ℃$, $\tau = \pm 50$℃, and T_H=100℃ and $A_\mathrm{p} = 0.9$A, which satisfy condition (C1).

When $L = \frac{1}{2} \cdot \lambda(T_0)$ and $\tau = -50$℃

$$\mathrm{i}\,\omega A^2 Z_\mathrm{a}(\mathrm{i}\omega) = (0.0015 + 1\mathrm{i})\omega d_\mathrm{a}$$

When $L = \frac{1}{2} \cdot \lambda(T_0)$ and $\tau = 50$℃

$$\mathrm{i}\,\omega A^2 Z_\mathrm{a}(\mathrm{i}\omega) = (-0.026 + 1\mathrm{i})\omega d_\mathrm{a}$$

In this case, considering an imaginary value of *i*1, the real parts are 0.0015 and -0.026, respectively, which are sufficiently small to be neglected. Thus, $\frac{C(T_0)}{0.6(T_H - T_0)} \cdot \ln\left|1 + \frac{0.6(T_H - T_0)}{C(T_0) + 0.6\tau}\right| \cong 1$.

D. Electrical impedance of the piezo-sounder

The electric impedance of the piezo-sounder is as follows [14]:

$$Z_e(\mathrm{i}\omega) = \frac{-m\omega^2+k+\mathrm{i}\omega D}{\mathrm{i}\omega C\left\{-m\omega^2+k+\frac{1}{2C}\left(\frac{Q}{d}\right)^2+\mathrm{i}\omega D\right\}} \qquad (8)$$

which includes the electrical as well as the mechanical elements (such as the mass, spring constant, and damper) of the vibrating plate and the air in the sounder cavity. According to the description provided in section *C* of this chapter, when the acoustic tube is connected to the sounder, as shown in Fig.1, the viscosity component, given by $\mathrm{i}\omega d_{\mathrm{a}} = \mathrm{i}\omega \frac{\rho(T_0)C(T_0)}{A_{\mathrm{p}}}A^2$ in eq.(5), is substantial in the temperature range of condition (C1). This factor is added to the impedance of the sounder and expressed as follows:

$$Z_{\mathrm{e}}(\mathrm{i}\omega) = \frac{-m\omega^2+k+\mathrm{i}\omega\left(D+\frac{\rho(T_0)C(T_0)}{A_{\mathrm{p}}}A^2\right)}{\mathrm{i}\omega C\left\{-m\omega^2+k+\frac{1}{2C}\left(\frac{Q}{d}\right)^2+\mathrm{i}\omega\left(D+\frac{\rho(T_0)C(T_0)}{A_{\mathrm{p}}}A^2\right)\right\}} \qquad (9)$$

After connecting the tube, the resonance and anti-resonance frequencies of the piezo-sounder are slightly influenced by the viscosity characteristics and mass and the spring characteristics when the temperature deviates from the reference. However, they are assumed to be same as those of the system with the sounder alone. Thus, they are as follows:

$$f_{\mathrm{r}} = \frac{1}{2\pi}\sqrt{\frac{k+\frac{1}{2C}\left(\frac{Q}{d}\right)^2}{m}} \qquad (10)$$

$$f_{\mathrm{ar}} = \frac{1}{2\pi}\sqrt{\frac{k}{m}} \qquad (11)$$

However, the damping coefficient is directly influenced by the acoustic viscosity $d_{\mathrm{a}} = \frac{\rho(T_0)C(T_0)}{A_{\mathrm{p}}}A^2$ and expressed as follows:

$$\zeta = \frac{1}{2}\frac{D+\frac{\rho(T_0)C(T_0)}{A_{\mathrm{p}}}A^2}{\sqrt{m\cdot\left(k+\frac{1}{2C}\left(\frac{Q}{d}\right)^2\right)}} \qquad (12)$$

The damping coefficient ζ is inversely proportional to the area A_{p} through which air can pass, which is inversely proportional to the bulk density of the objects. Thus, using double negation, the damping coefficient ζ is proportional to the bulk density of the objects, as shown in Fig.3.

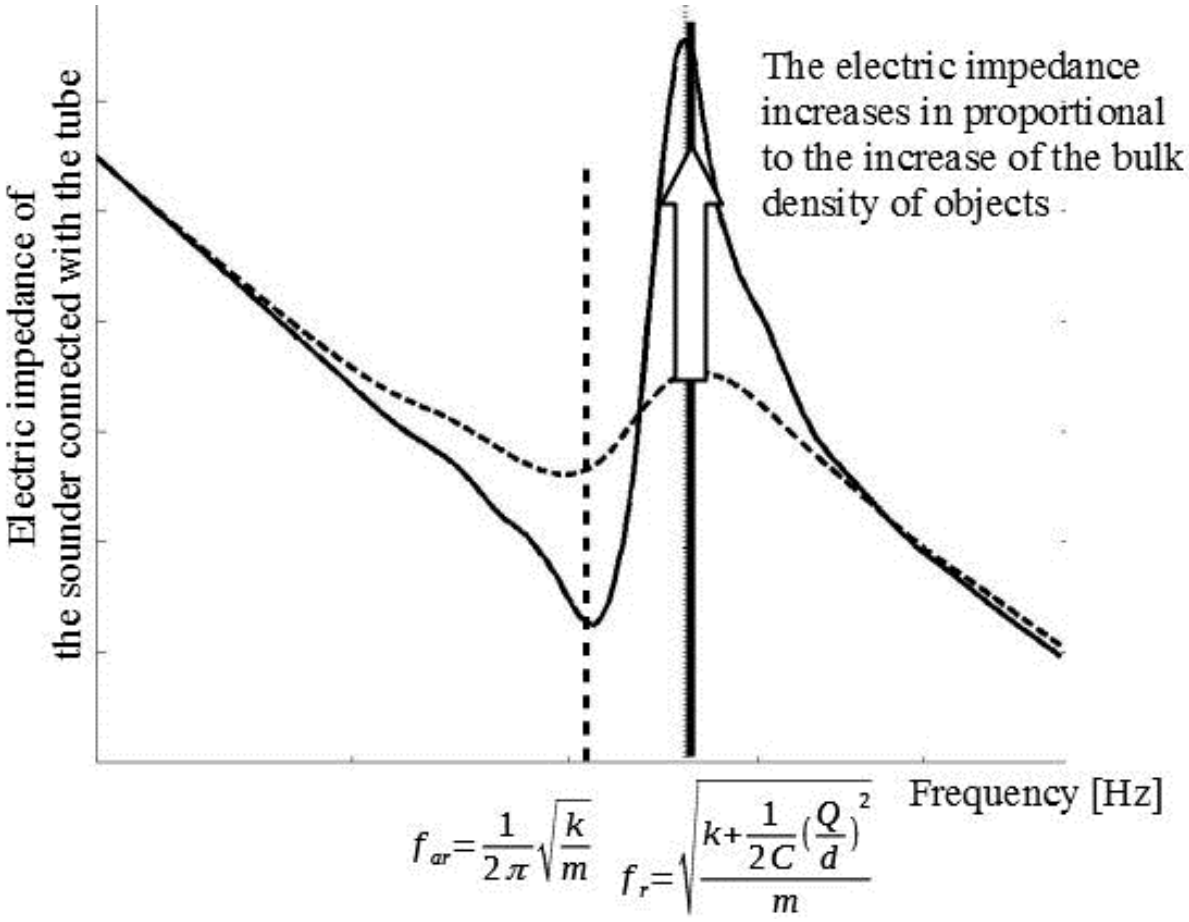

Fig.3 Frequency response of the impedance when the detection position is covered and open.

4.3 EXPERIMENTAL VERIFICATIONS

A. Verification of theoretical results

Here, we investigate the electric impedance of a piezo-sounder connected with the acoustic tube under various environmental temperatures and compare the theoretical results with the experimental results. Figure 4 shows the sounder and the tube, which is inside the tank. The tube and the air inside it were heated or cooled by pouring hot water or placing ice blocks into the tank. The piezo-sounder (Murata PKM44EW) had a resonance frequency of 760 Hz. The radius of the acoustic tube was 7 mm and its length was 0.22 m, which was the half-wavelength with open-end compensation 0.6×7 mm, 760 Hz sound, and a temperature of 16°C.

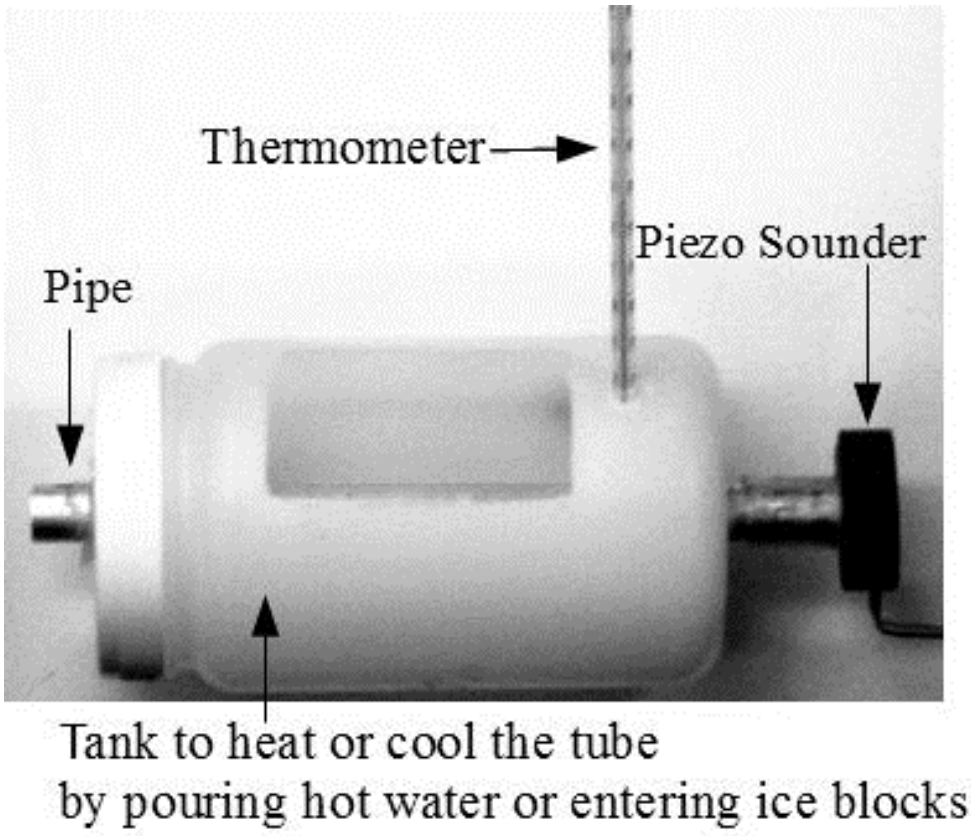

Fig.4 Experimental set-up used to measure the electrical impedance of a sounder connected with the acoustic tube

First, hot water of 90°C was poured into the tank, and the temperature gradually deceased by heat radiation. When the temperature decreased to approach room temperature, the water was further cooled to 5°C by inserting ice blocks into the tank. The frequency response of the electric impedance was measured at several temperatures using a spectrum analyzer (Digilent 410-321). The electric impedance was determined by dividing the sounder terminal voltage by the current. The frequency range was 500 Hz to 1 kHz, which included the resonance and anti-resonance frequencies. The detection port was closed by covering it with cotton of bulk density 36 kg/m^3, which is approximately 30 times higher than that of air. Figure 5 shows the frequency responses of the impedance of the sounder when the port was open and closed; for example, at temperatures of 5°C, 40°C, and 80°C. In the open condition, the impedance had a maximal value near the resonance

frequency for all temperatures. The maximal value of the impedance at a low temperature of 5°C and a high temperature of 80°C decreased compared to that observed at approximately 40°C.

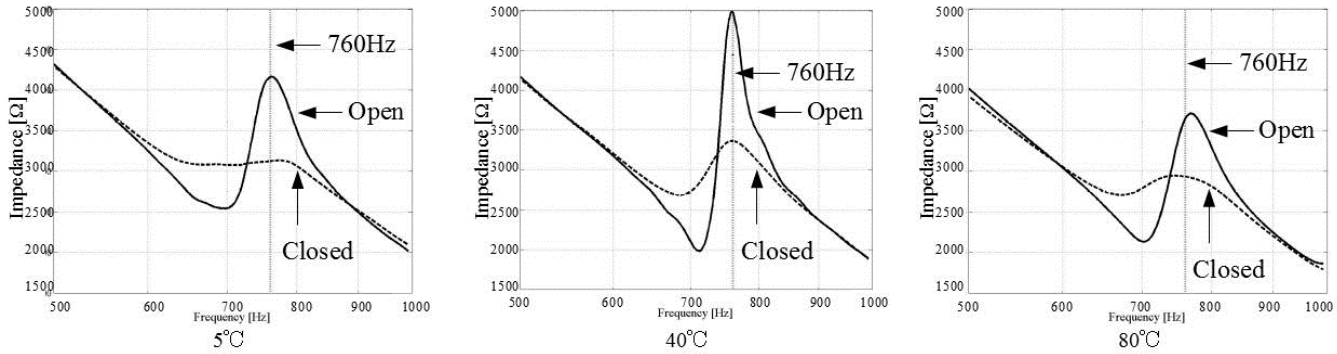

Fig.5 Frequency response of the electric impedance of the sounder when the detection point is open or closed with cotton of bulk density 36 kg/m^3 in the temperature range 5°C–80°C

However, the electric impedances of the closed condition were flat for the entire temperature range examined in the experiment and were lower than those measured in the open condition. Throughout the studied temperature range, the frequencies of the open condition impedance were observed as maxima and ranged from 753 Hz to 766 Hz and the average frequency was 758 Hz. At the anti-resonance frequency, the impedances of the closed condition were greater than those of the open condition.

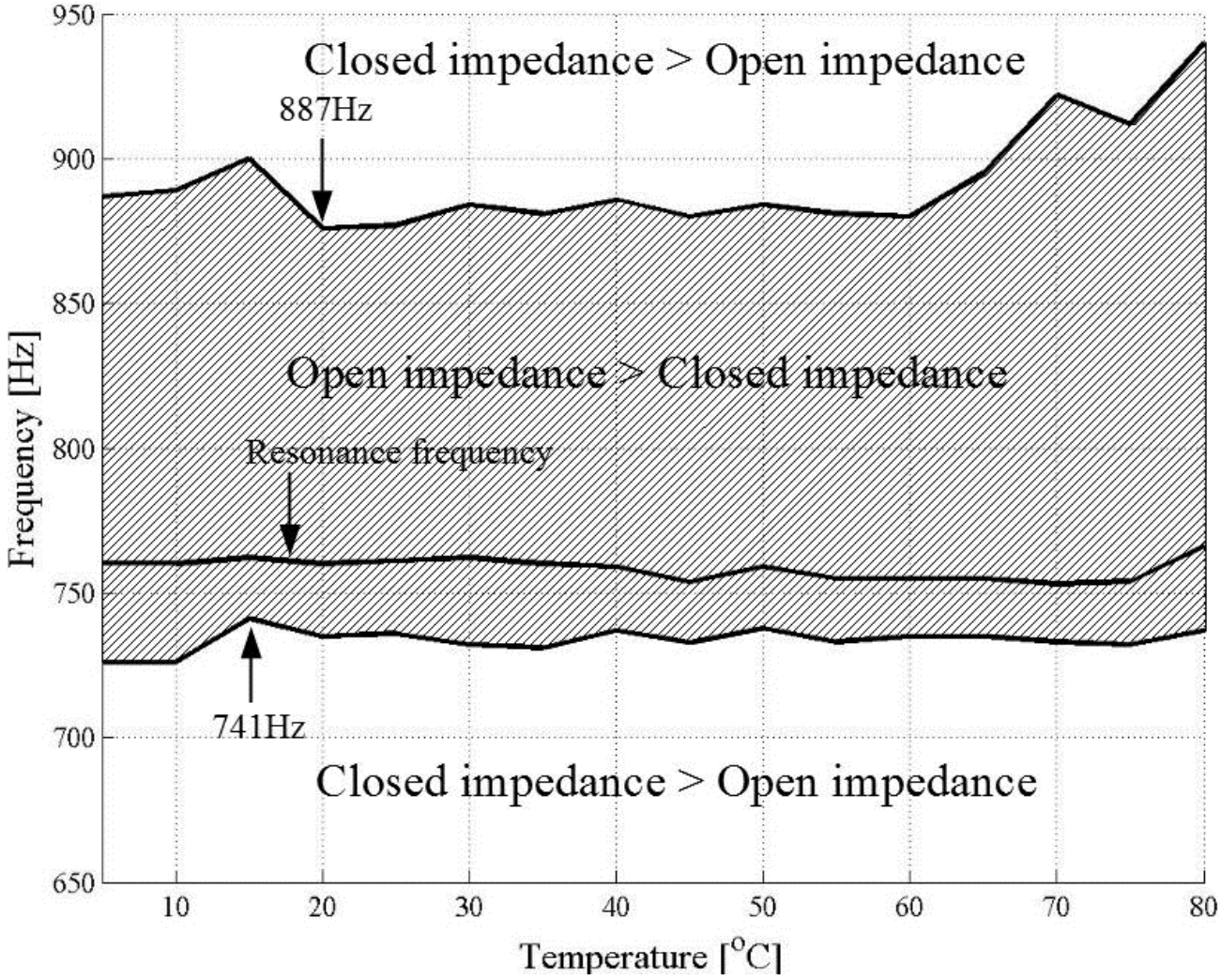

Fig.6 Frequency range for which the open resonance impedance is greater than the closed impedance; resonance frequency for temperature ranging from 5°C to 80°C

Figure 6 shows the frequency range when the impedance of the open condition is greater than that of the closed condition, as well as the resonance frequency for the temperature range from 5°C to 80°C.

From Fig.6, the highest frequency of the lower frequency limit is 741 Hz and the lowest frequency of the upper frequency limit is 877 Hz. The standard deviation for the resonance frequency 758 Hz was 4Hz; thus, the resonance frequency was almost constant for changing temperature.

Figure 7 shows the acoustic impedance of the piezo-sounder and the output voltage $e(t)$ of Fig.1 at a constant frequency of 760 Hz for a temperature ranging from 5°C to 80°C.

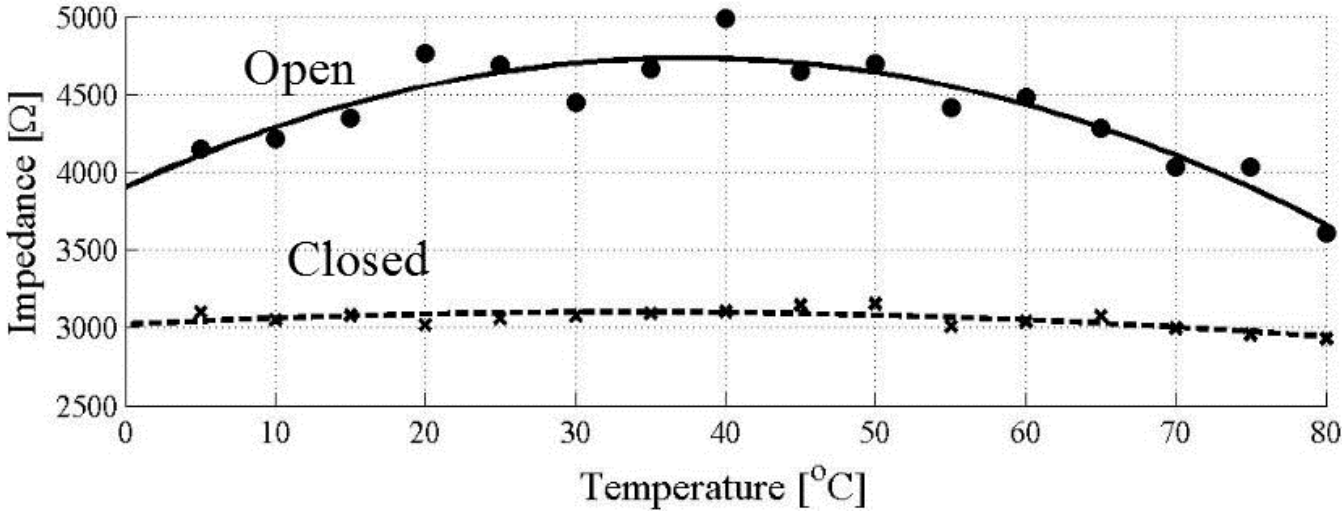

(a) Temperature vs. impedance

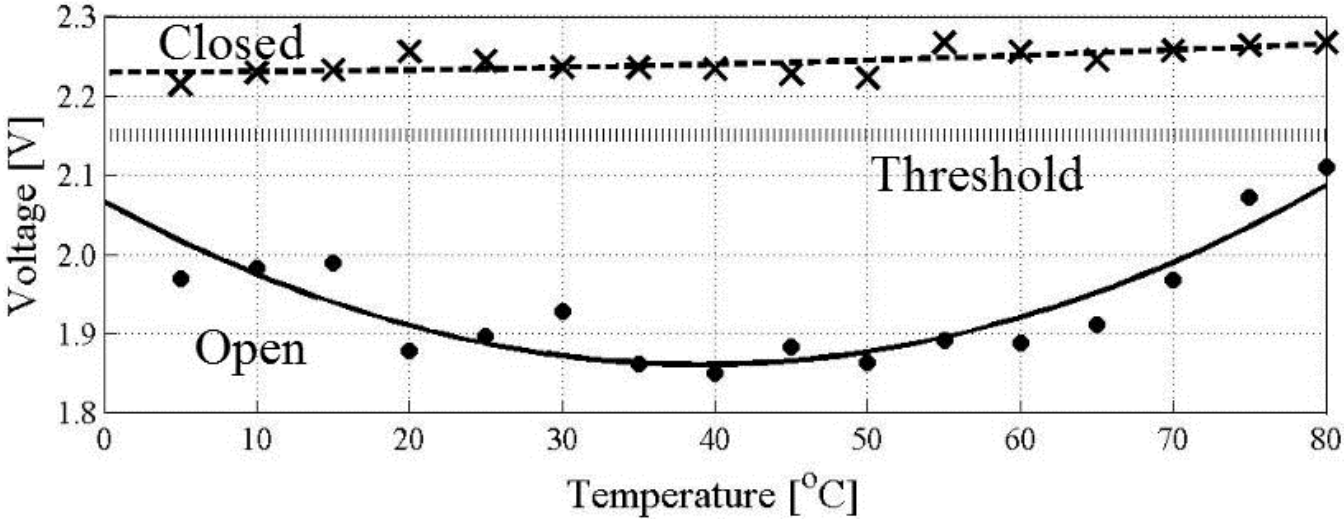

(b) Temperature vs. output voltage

Fig.7 Open and closed resonance impedances for temperature ranging from 5°C to 80°C

The impedance measured in the closed condition is almost constant for the entire temperature range, whereas that observed in the open condition decreases when the temperature is lower or higher than room temperature. The output voltage shows the inverse characteristics to the impedance. In this case, setting a fixed threshold of 2.15 V can judge the open or closed condition.

B. Detectable bulk density of objects

Figure 8 shows the bulk density of an object as a function of the output voltage when the environmental temperature is 23°C. The object employed here was cotton with bulk density ranging from 13 kg/m^3 to 70 kg/m^3 and the port was covered with cotton with bulk density 13 kg/m^3; the output voltage was 1.9 V, which was the lowest detectable limit.

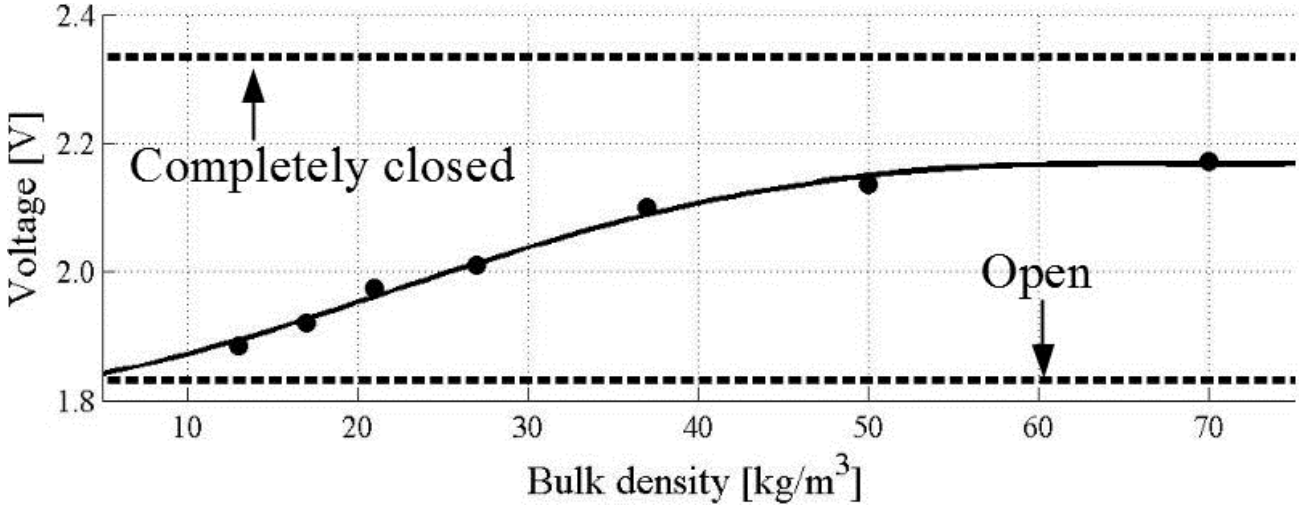

Fig.8 Bulk density vs. output voltage

C. Effect of a dust filter placed at the quarter-wavelength position

At the quarter-wavelength position of the tube, the amplitude of the sound velocity is minimal or coincides with the node location of the sound velocity. Thus, the kinematic energy lost by the air filter plugging is minimal, which leads to lower influence to the acoustic resonance. This was verified experimentally. For a tube with length 0.22 m, we placed a dust filter at the quarter-wavelength location, 0.11 m. The dust was substituted by cotton of 36 kg/m^3 bulk density attached to the filter. The environmental temperature was 23°C. The detection port was closed by covering it with cotton of the same bulk density as that of the dust cotton. Figure 9 shows the dust and output voltages when the detection port was open and covered by cotton as a function of dust (cotton) thickness. From Fig.9, even when the tube was plugged by 26.5-mm-thick dust, the method detected the existence of the object (cotton). Furthermore, when the environmental temperature did not change, from the output voltage of the open condition, the thickness of the dust could be estimated, which could generate a message to clean the filter.

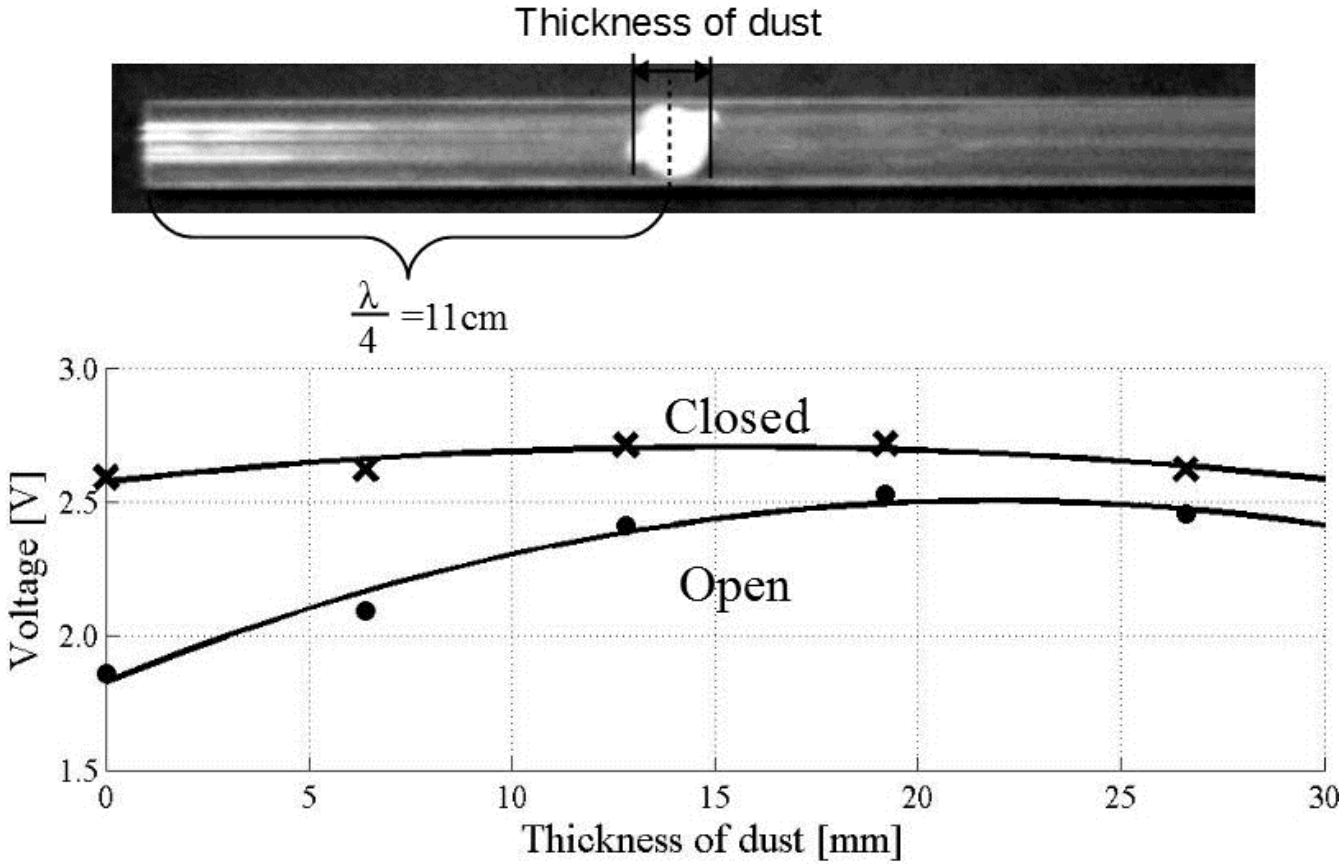

Fig.9 Effect of the thickness of the dust attached to the dust filter

D. Dust blow-out phenomena at the detection port

Because the tube length was the half-wavelength, at the open detection port, the amplitude of the sound velocity of the air, and thus its kinetic energy, was maximum; this is sufficiently large to remove the dust around the detection port. The force required by the piezo-sounder to draw air from the exterior of the detection port is lower than that required to extract it from the tube. Because the air pushes out, diverges, and scatters into space and a part of the scattered air is pulled into the port. Thus, the resulting force acting on the dust is directed toward the exterior of the tube, which blows out the dust near the detection port and maintains the interior of the tube clean. Figure 10 shows this phenomenon. When the sounder was driven by 3.6 mV. First, 100 Styrofoam balls with 3.0 mm diameter and with group bulk density of 10 kg/m^3 were placed inside and near the detection port of the tube horizontally. The air gradually pushed the balls against the friction force between the balls and the tube surface and extracted them all from the tube after 45 s. From Fig.10, it is evident that the tube has the capability to blow out dust located around the detection port.

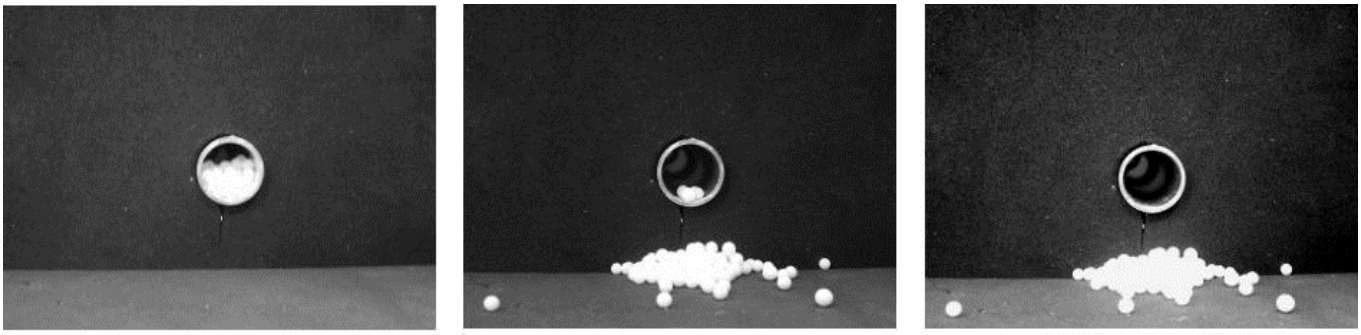

Fig.10 Dust blown out by acoustic energy

E. Switching under changing environmental temperature

We performed an experiment using a level switch based on the scheme shown in Fig.1 under the same experimental conditions as those shown in Fig.4. Here, we employed the dynamic-threshold logic presented in Fig.1 with parameters e_t = 2.2 V, t_j = 10 s, and ε = 0.1 V. The sampling interval of the AD converter was 1 ms. In a 8000 s period, the detection port was covered (using cotton with bulk density 36 kg/m^3) and opened every other 120 s and the temperature changed from 90°C to 5°C. Figure 11 shows the observed switching behavior and environmental temperature. The temperature was changed in the same way as in the verification experiment described in section A of this chapter. During the time interval, all switching was correctly estimated. The voltage difference between the open and closed conditions in the temperature range from 5°C to 90°C was almost the same.

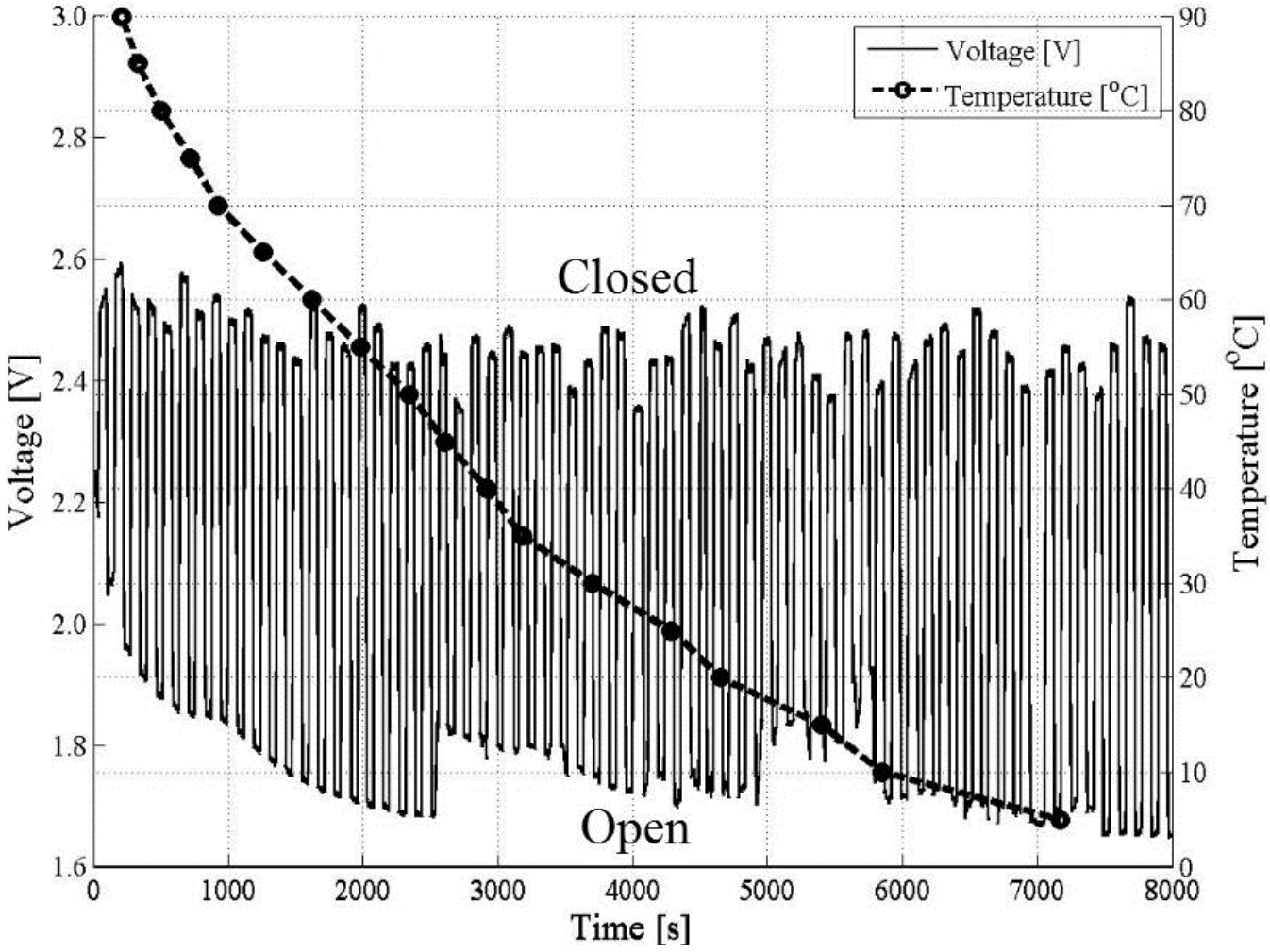

Fig.11 Level switching when the environmental temperature changes from 90°C to 5°C

F. Experimental detection of hot soil

Using a stainless tube of length $L \cong 0.900$m, which is equal to two wavelengths, we performed an experiment to detect the presence of heated gravel with a bulk density of 810 kg/m^3. Figure 12 shows the temperature of the gravel and the tube. The highest surface temperature of the heated gravel was 345°C and its interior temperature was 450°C. The surface temperature was measured with a thermo-tracer camera (Japan Avionics F30) and the internal temperature was measured with an optical thermometer (CUSTOM CT-2000D). The temperature distribution along the tube was 32.1°C, 30.2°C, 30.3°C, 29.8°C, and 29.7°C beginning from the gravel side. The stainless tube functioned not only as an acoustic tube but also as a heat-radiation tube.

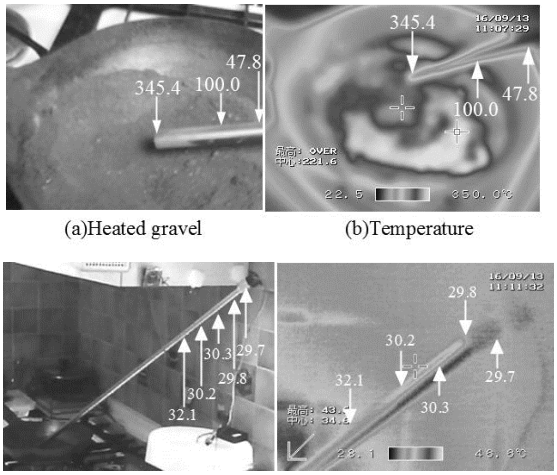

Fig.12 Temperature of the heated gravel and temperature distribution along the acoustic tube

Figure 13 shows that the output voltage was 2.5 V when the detection port was covered with the hot gravel, and 0.9 V when the gravel was removed. The presence of the heated gravel was correctly assessed using a constant threshold of 2.2 V.

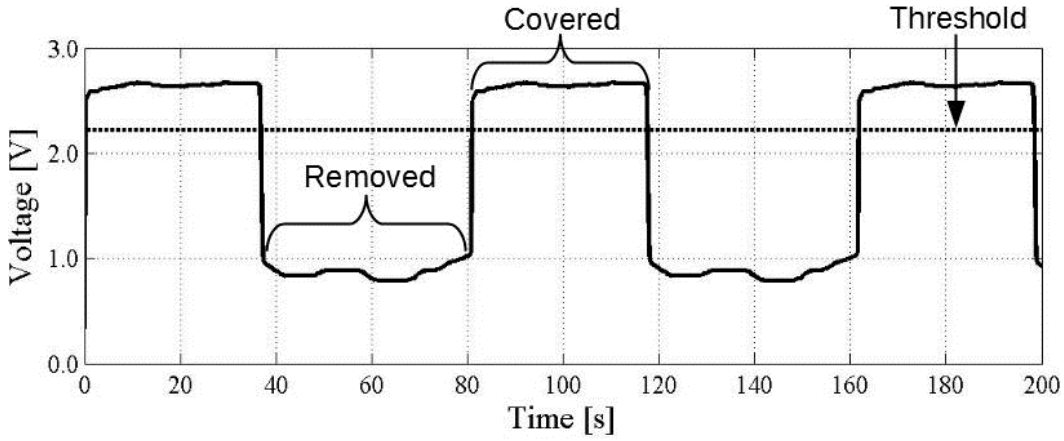

Fig.13 Change in the output voltage observed when the detection port was covered by heated gravel three times

4.4 RESULTS

Here, we summarize the results of the experiments described in Chapter III.

An acoustic tube with 7 mm radius and 0.22 m length, which is the half-wavelength of a 760 Hz sound at 19°C, was acoustically excited by a sounder with a resonance frequency of 760 Hz. The detection port was covered with cotton and then uncovered. The bulk density of the cotton was 36 kg/m^3. When the environmental temperature changed from 5°C to 80°C, we obtained the following results:

(R1) In the frequency range from 740 Hz to 874 Hz, the electric impedance of the sounder was greater when the detection port was open than when it was covered or closed.

(R2) When open, the resonance frequency was 758±4 Hz, and the difference between the impedances of the closed and open conditions was maximum at the resonance frequency.

(R3) When the half-wavelength was equal to the length of the tube, the temperature was optimal. At this optimal temperature, the difference between the impedances of the closed and open conditions was maximum. Even when deviating from the optimal temperature condition (± 50℃), the open and closed conditions were correctly evaluated by using a fixed threshold.

(R4) Under a constant temperature condition, the detectable bulk density of powders (cotton) was 13 kg/m^3.

(R5) Even when a dust filter placed at the quarter-wavelength position of the tube was plugged with 26.5-mm-thick dust (cotton) with 36 kg/m^3 bulk density, the method detected the presence of the powder (cotton) with the same bulk density as that of the dust. Furthermore, when the detection port was open, the output voltage increased proportionally to the thickness of the dust.

(R6) The acoustic tube had the capability of blowing out dust accumulated inside and near the detection port.

(R7) In an environment with varying temperature from 90°C to 5°C, the dynamic-threshold logic correctly identified the presence of a powder (cotton) of 36 kg/m^3 bulk density.

(R8) Under the different conditions described above, the 0.90-m-long acoustic tube detected the presence of gravel with bulk density 810 kg/m^3 heated from 345°C to 450°C.

4.5 CONSIDERATIONS

From the results (R1) and (R2), the objects (in the experiment the cotton) that satisfied condition (C2) had little influence on the resonance frequency of the piezo-sounder. The results confirmed that the air in the acoustic tube functions not mass or spring but viscosity. This result corresponds to the theoretical results given by eq.(4), (5), (10), (11), (12), and Fig.3. From result (R3), even with an environmental temperature deviation of ±50℃ from the optimal temperature, the open and closed conditions can be determined.

Two common problems of powder-level meters is dust fixing by condensation and the drying of dew that contains dust. In this method, we placed a dust filter at the quarter-wavelength (namely, at the position of the loop of the sound pressure or the node of the sound velocity) that had little influence on acoustic phenomena and obtained result (R5). Furthermore, the acoustic tube driven by the sounder had the capacity to blow out dust from the vicinity of the detection port.

4.6 CONCLUSIONS

In this paper, we propose a novel acoustic-tube level switch that detects the level of light and hot powders or fibers in a tank. A mathematical model was build and the influence of the environmental temperature was theoretically investigated. From this investigation, we determined that the optimal length of the acoustic tube for a certain temperature still operates well for a temperature deviation of ±50℃ from the optimal temperature. Experimentally, the proposed level switch evaluated the level for the temperature range from 5℃ to 90℃ or a wider temperature range under a fixed evaluation threshold. The acoustic method, which has been considered to be easily influenced by temperature changes, was observed to be robust against such changes. The temperature variation of the exterior of the tank was within ±50℃ from the reference temperature, it is feasible. Furthermore, when we used the dynamic-threshold logic shown in Fig.1, the system could operate in a wider temperature range than ±50℃. The main feature of the method is that it can detect light powders. Experimentally, we confirmed that the method can detect a fibrous substance (cotton) of 15 kg/m^{3}bulk density, which is approximately ten times higher than the atmospheric air density. A filter set at the quarter-wavelength position had little influence on the acoustics, even when 26.5-mm-thick dust was plugged. Furthermore, an acoustic tube driven by a sounder could blow out dust from the vicinity of the detection port. Finally, by using the acoustic tube as a heat radiator, we can detect gravel heated to approximately 450℃. The proposed method can be used in the ash-processing plants of garbage incinerators or in bubble level detectors in savior environmental conditions.

Here, we described the simplest acoustic level switch with a constant length tube driven by a piezo-sounder at a constant frequency. Although the level switch had the simplest structure, it was sufficiently robust against changes in the temperature and dust. A variety of advanced schemes can be considered based on the proposed method.

REFERENCES

[1] Committee of federation of industrial instrument in Japan, “ Level meter,” federation of industrial instrument in Japan, 1993

[2] S.S. Novikov, A.S., Maidanovskii, A.P., Rostov, Yu, M. Andreev : ”Microwave level meter with wire line,” KORUS’99, pp.661-662, 1999

[3] M. Norhisam, H. Ezril, M. Senan, N. Mariun, H. Wakiwaka, and M. Nirei, ”Positioning System for Sensor-less Linear DC Motor,” First International Power and Energy Conference PECON 2006 November 28-29, Putrajaya, Malaysia, pp.476-481

[4] M. Vogt, M. Gerding, T. Musch, "Implementation and evaluation of coherent synthetic aperture radar processing for level measurements of bulk goods with an FMCW system", Adv. Radio Sci., vol. 8, pp. 7-11, 2009

[5] M. Vogt, M. Gerding, V. Fortoul, “ An optimized radar system for tank level measurement in dispersive bypass pipes,” 2015 German Microwave Conference pp.178-181, 2015

[6] E.J. Chern and B.B. Djordjevic, "Nonintrusive ultrasonic low-liquid-level sensor," Mater. Eval. Vol. 48, no. 4, pp. 481-485, 1990

[7] Eldar Musayev and Sait Eser Karlik, "A novel liquid level detection method and its implementation," Sensors and Actuators A, vol. 109, pp. 21-24, 2003

[8] Zhen Chen, Gerald Hefferman and Tao Wei, "Multiplexed Oil Level meter Using a Thin Core Fiber Cladding Mode Exciter, “IEEE PHOTONICCS TECHNOLOGY LETTERS, VOL.27, NO.21, 2015

[9] M. Vogt, T. Neumann, M. Gerding, "Frequency-diversity technique for reliable radar level measurement of bulk solids in silos", European Radar Conf., pp. 129-132, Oct. 2013

[10] M. Vogt, T. Neumann, M. Gerding、"Silo and Tank Vision", IEEE Microwave Magazine pp.38-51(2017)

[11] Dietmar Schultze, “Powders and Bulk Solids –Behavior, Characterization, Storage and Flow-“, Springer 2007

[12] A. Ooshima, K.Kobyashi and K. watanabe,”Development of noninvasive powder level switch by acoustic method”, SICE Annual Conf. in Sapporo August 4-6 (2004)

[13] T. Yoshida, K. Kobayashi, K Suzuki, K. Yamashita and K. Watanabe, “Acoustic Tube Level Switch for Particles”, SICE Trans. 10-1,pp.1-9 (2017)

[14] T. Yoshida, K. Kobayashi, Y. Kurihara, N. Shiroi, and K. Watanabe, “Multiple-Input/Multiple-Output Characteristics of Piezo Devices and an Application for Triage,” IEEE Sensors Journal Vo.17, Issue 5 pp.1434/1442, (2017)

5. Conclusion

We construct a comprehensive theoretical model of piezo device based on the piezoelectric effect, electrical property, mechanical property and pyroelectric effect of piezo device, and derived a system block diagram to express the physical modeling. We revealed that the reversible phenomenon is due to feedback. Moreover, the structure of multiple input / multiple output characteristics of piezo device was clarified by the structure that various physical quantities are applied to this feedback loop. By understanding the physical structure of this piezo device, the possibility of various multi-input and output function is introduced.

5.1 Multiple-Input/Multiple-Output Characteristics of Piezo Devices

The multi-input / multi-output characteristics of the piezo device was explained by feedback system which is inherent in the electrical and mechanical elements relation. In addition, the reversibility characteristic of the piezo device was also explained based on this feedback theory. From the derived feedback block model, we introduce considerable various new application of the piezo device.

The piezo ceramic device was reviewed from the internal physical phenomenon and modeling was introduced. From the derived block diagram model, we found that the piezo device has inherent feedback loop swhich can be reversely operated. Some of piezo ceramic elements composed of ferroelectrics had not only piezoelectric effects but also pyroelectric properties, and experiments showed that temperature differences can be detected by experiments.

5.2 Respirometer by a piezo device and its application to triage

Based on a new insight from chapter 2, we developed a new triage support device using the pyroelectric effect of the piezo device and the feedback characteristics in the element. The proposed triage support device is used as two sides of the piezo device, such as (1) respiration sensor, (2) as a buzzer. In the normal condition, proposed triage support device detects as a respiration sensor. However, when an abnormality is detected in respiration, the triage support device act as a buzzer to warn for the triage. This function can be realized with a power-saving microprocessor and a single piezo device as a dual function of sensor and actuator.

The proposed triage support device demonstrate new possibilities in the field of medical engineering not only as a triage sensor but also simple respiration sensor.

5.3 Powder and Bulk Level Monitoring by an Acoustic Tube Method

We developed a level switch that utilizes a piezo device as a sound generating mechanism to drive the Helmholtz cavity and acoustic tube and detects whether the tip of the acoustic tube is covered with an object having a light bulk density from the piezo device impedance change. The proposed acoustic level switch demonstrates a capability of variety of new industrial field instruments.

We studied acoustic tube level switch which detects the existing of powder / granular material with low bulk density. A mathematical model of acoustic tube was constructed and the temperature dependency of this system was theoretically explained. In other words, the optimum design of the acoustic system (constant acoustic tube length and actuated sound

frequency) optimally designed under a certain temperature disintegrates with the temperature change, however it is still possible to detect as level switch. As a result, it was theoretically confirmed that discrimination was made normally at the optimum condition temperature ± 50 ° C, experimentally it was determined with a fixed threshold in the temperature range 5 to 80 ° C with robustness and robust to temperature was confirmed. The temperature outside the tank of the proposed level switch is within ± 50 ° C at room temperature and can be examined as practical situation. In addition, even if the temperature further changes by the dynamic threshold method, it can deal without false detection. Regarding the bulk density, we confirmed that 13 kg / m 3 of cotton can be discriminated. It was confirmed that the level of adhesion of dust on the dustproof filter can be monitored and information on filter replacement can be outputted. Finally, using the fact that the sound tube acts as a heat radiation pipe, the presence or absence of dirt at a temperature of 345.4 to 450 ° C can be stably switched regardless of temperatures change. Such a level switch can be expected to be effective for detection of low bulk density objects in an adverse environment, such as ash treatment process of garbage incineration plants and bubble level detection of food / water treatment plants.

APPENDIX

Fig.A1 shows a cylindrical tube with uniform cross-sectional area. Here, we consider its acoustic characteristics.

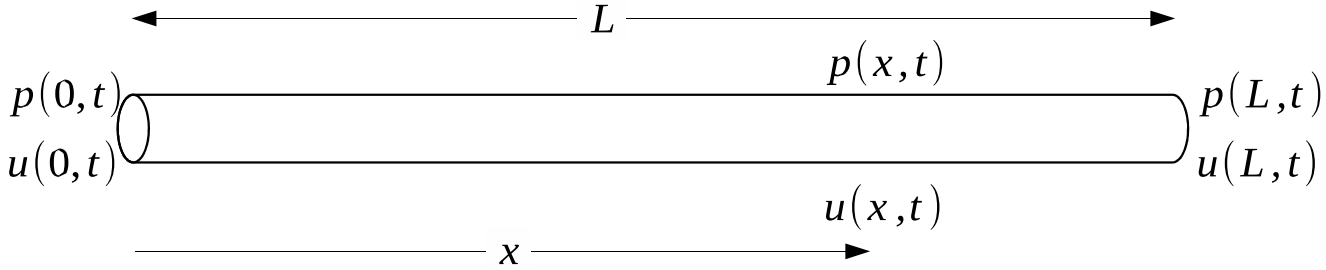

Fig.A1 Cylindrical acoustic tube with uniform cross-sectional area

The acoustic wave propagation in the tube is described by the following wave equations, eq.(A1) and eq.(A2) [11].

$$-\frac{\partial u(x,t)}{\partial t}=\frac{A}{\rho(T)}\frac{\partial p(x,t)}{\partial x} \qquad \text{(A1)}$$

$$-\frac{\partial p(x,t)}{\partial t}=\frac{\rho(T)\cdot(C(T))^2}{A}\frac{\partial u(x,t)}{\partial x} \qquad \text{(A2)}$$

In these equations, the air density $\rho(T)$ and sound velocity $C(T)$ are a function of the temperature T and are expressed as follows:

$$\rho(T)=\frac{1.239\times P}{1+T/273.15} \qquad \text{(A3)}$$

$$C(T)=331.5\text{m/s}+0.6T \qquad \text{(A4)}$$

As the change of the temperature is very slow in comparison with the acoustic phenomena, the temperature is assumed to be constant. Under this condition, the solution of the ordinary differential equation with respect to the displacement x, obtained by the Laplace transformations of eq.(A1) and eq.(A2) for zero initial conditions, are given in the form of the following four terminal network relations

$$\begin{bmatrix}P(x,s)\\U(x,s)\end{bmatrix}=\begin{bmatrix}\cosh\frac{s}{C(T)}x & -\frac{\rho(T)C(T)}{A}\sinh\frac{s}{C(T)}x\\ -\frac{A}{\rho(T)C(T)}\sinh\frac{s}{C(T)}x & \cosh\frac{s}{C(T)}x\end{bmatrix}\begin{bmatrix}P(0,s)\\U(0,s)\end{bmatrix} \qquad \text{(A5)}$$

When the tube is driven by a steady-state sinusoidal sound with angular frequency ω, the relation in eq.(A5) is expressed as follows:

$$\begin{bmatrix}P(x,i\omega)\\U(x,i\omega)\end{bmatrix}=\begin{bmatrix}\cos\frac{\omega}{C(T)}x & -i\frac{\rho(T)C(T)}{A}\sin\frac{\omega}{C(T)}x\\ -i\frac{A}{\rho(T)C(T)}\sin\frac{\omega}{C(T)}x & \cos\frac{\omega}{C(T)}x\end{bmatrix}\begin{bmatrix}P(0,i\omega)\\U(0,i\omega)\end{bmatrix} \qquad \text{(A6)}$$

From condition (C1), the temperature distribution $T(x)$ along the tube is as shown in Fig.A2 and given by eq.(A7)

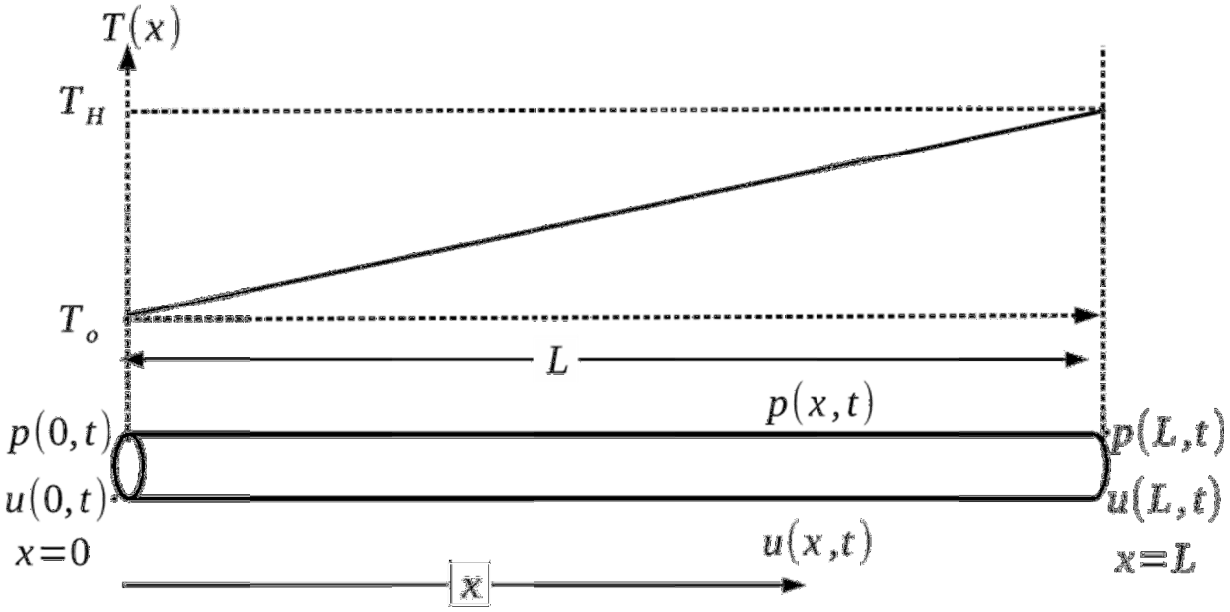

Fig.A2 Linear temperature distribution along the acoustic tube

$$T(x) = T_o + \frac{T_H - T_o}{L}x \qquad \text{(A7)}$$

In the tube, the length of a short part of the tube is given by Δx and the total length of the tube is divided into $m = L/\Delta x$ parts. Here, we define the angle $\theta(k) = \frac{\omega \Delta x}{C(T(k\Delta x))}$ for the short tube. From eq.(A4) and eq.(A7), the angle $\theta(k)$ at the k-th tube is given as follows:

$$\theta(k) = \frac{\omega \Delta x}{331.5 + 0.6\left(T_o + \frac{T_H - T_0}{L}k\Delta x\right)} = \frac{\omega}{C(T_0)} \cdot \frac{\Delta x}{1 + \frac{0.6(T_O) + \frac{T_H - T_0}{L}k\Delta x}{C(T_0)}} \qquad \text{(A8)}$$

and the four terminal matrices of the k-th tube from $k\Delta x$ to $(k+1)\Delta x$ are obtained from eq.(A6).

$$F(k\Delta x) = \begin{bmatrix} \cos\theta(k) & -i\frac{\rho(T(k\Delta x))C(T(k\Delta x))}{A}\sin\theta(k) \\ -i\frac{A}{\rho(T(k\Delta x))C(T(k\Delta x))}\sin\theta(k) & \cos\theta(k) \end{bmatrix} \qquad \text{(A9)}$$

Thus, the acoustic characteristics from $k\Delta x$ to $(k+1)\Delta x$ are expressed as follows:

$$\begin{bmatrix} P((k+1)\Delta x, i\omega) \\ U((k+1)\Delta x, i\omega) \end{bmatrix} = F(k\Delta x)\begin{bmatrix} P(k\Delta x, i\omega) \\ U(k\Delta x, i\omega) \end{bmatrix} \qquad \text{(A10)}$$

The characteristics of the entire tube from $x = 0$ to $x = L$ are given by the products of $F(0), F(\Delta x), \ldots F(k\Delta x), \ldots, F(m\Delta x)$, which are expressed as follows:

$$\begin{bmatrix} P(L, i\omega) \\ U(L, i\omega) \end{bmatrix} = \prod_{k=1}^{m} F(k\Delta x)\begin{bmatrix} P(0, i\omega) \\ U(0, i\omega) \end{bmatrix} \qquad \text{(A11)}$$

From condition (C1), the temperature difference between T_{H} and T_{o} is approximately 100°C; from eq.(A3) and (A4), in the temperature range 0°C $\leq T \leq$ 100°C with central temperature $T = \frac{T_H + T_o}{2} = 50$℃, the maximum deviation is approximately ±4%, which yields the following approximation

$$\rho(T_{\mathrm{o}})C(T_{\mathrm{o}}) \cong \rho(T)C(T) \cong \rho(T_{\mathrm{H}})C(T_{\mathrm{H}}) \qquad \text{(A12)}$$

Using the approximation above and the additional theorem of the trigonometric function, we have:

$$\prod_{k=1}^{m} F(k\Delta x) = \begin{bmatrix} \cos\sum_{k=1}^{m}\theta(k) & -i\frac{\rho(T_o)C(T_o)}{A}\sin\sum_{k=1}^{m}\theta(k) \\ -i\frac{A}{\rho(T_o)C(T_o)}\sin\sum_{k=1}^{m}\theta(k) & \cos\sum_{k=1}^{m}\theta(k) \end{bmatrix} \text{(A13)}$$

Furthermore, by letting $\Delta x \to 0$ the angle $\theta = \sum_{k=1}^{m} \theta(k)$ is calculated as follows:

$$\theta = \lim_{\Delta x \to 0} \sum_{k=1}^{m} \theta(k) = \frac{\omega}{C(T_\mathrm{o})} \lim_{\Delta x \to 0} \sum_{k=1}^{m} \frac{\Delta x}{1 + \frac{0.6(T_\mathrm{H} - T_\mathrm{o})}{C(T_o)L} k\Delta x}$$

$$= \frac{\omega}{C(T_o)} \int_0^L \frac{dx}{1 + \frac{0.6(T_\mathrm{H} - T_\mathrm{o})}{C(T_\mathrm{o})L} x} = \frac{\omega L}{0.6(T_\mathrm{H} - T_\mathrm{o})} \ln \left| 1 + \frac{0.6(T_\mathrm{H} - T_\mathrm{o})}{C(T_\mathrm{o})} \right| \quad \text{(A14)}$$

Then, when the environmental temperature deviates by τ from T_0, the angle $\theta(\tau)$ can be described as:

$$\theta(\tau) = \frac{\omega L}{0.6(T_\mathrm{H} - T_\mathrm{o})} \ln \left| 1 + \frac{0.6(T_\mathrm{H} - T_\mathrm{o})}{C(T_\mathrm{o}) + 0.6\tau} \right| \quad \text{(A15)}$$

Thus, the acoustic characteristics from $x = 0$ to $x = L$ in the temperature distribution of Fig.A2 are given by:

$$\begin{bmatrix} P(L, \mathrm{i}\omega) \\ U(L, \mathrm{i}\omega) \end{bmatrix} = \begin{bmatrix} \cos\theta(\tau) & -\mathrm{i}\frac{\rho(T_o)C_o(T_o)}{A} \sin\theta(\tau) \\ -\mathrm{i}\frac{A}{\rho(T_o)C_o(T_o)} \sin\theta(\tau) & \cos\theta(\tau) \end{bmatrix} \begin{bmatrix} P(0, \mathrm{i}\omega) \\ U(0, \mathrm{i}\omega) \end{bmatrix} \quad \text{(A16)}$$

Conversely, those from $x = L$ to $x = 0$ are given as follows:

$$\begin{bmatrix} P(0, \mathrm{i}\omega) \\ U(0, \mathrm{i}\omega) \end{bmatrix} = \begin{bmatrix} \cos\theta(\tau) & \mathrm{i}\frac{\rho(T_o)C_o(T_o)}{A} \sin\theta(\tau) \\ \mathrm{i}\frac{A}{\rho(T_o)C_o(T_o)} \sin\theta(\tau) & \cos\theta(\tau) \end{bmatrix} \begin{bmatrix} P(L, \mathrm{i}\omega) \\ U(L, \mathrm{i}\omega) \end{bmatrix} \quad \text{(A17)}$$

From condition (C2), the objects are acoustically viscous and the area that the air can pass through is A_p; thus, the viscosity resistance R_a can be obtained as:

$$R_\mathrm{a} = \frac{\rho(T_H)C(T_H)}{A_\mathrm{p}} \quad \text{(A18)}$$

Then, the acoustic volumetric velocity is given as follows:

$$U(L, \mathrm{i}\omega) = \frac{P(L, \mathrm{i}\omega)}{R_\mathrm{a}} \quad \text{(A19)}$$

From eq.(A18), eq.(A19), and eq.(A12) the acoustic impedance viewed the from $x = 0$ port is:

$$Z_\mathrm{a}(\mathrm{i}\omega) = \frac{P(0, \mathrm{i}\omega)}{U(0, \mathrm{i}\omega)} = \frac{\cos\theta(\tau) + i\frac{\rho(T_\mathrm{o})C(T_\mathrm{o})}{AR_a} \sin\theta(\tau)}{\frac{\cos\theta(\tau)}{R_\mathrm{a}} + i\frac{A}{\rho(T_\mathrm{o})C(T_\mathrm{o})} \sin\theta(\tau)} = R_a \frac{1 + \mathrm{i}\frac{A_\mathrm{p}}{A} \tan\theta(\tau)}{1 + \mathrm{i}\frac{A}{A_\mathrm{p}} \tan\theta(\tau)} \quad \text{(A20)}$$

The multiplication of A^2 with R_a leads to the following mechanical viscous coefficient

$$d_\mathrm{a} = A^2 R_a = \frac{\rho(T_H)C(T_H)}{A_\mathrm{p}} A^2 \quad \text{(A21)}$$

Furthermore, the operation of the time derivative iω on $Z_\mathrm{a}(\mathrm{i}\omega)$ with dimensions [Pa/(m^3/s)] yields the spring constant, which is given by a complex number with dimensions [N/s]:

$$\mathrm{i}\,\omega\, A^2 Z_\mathrm{a}(\mathrm{i}\omega) = \mathrm{i}\,\omega\, d_\mathrm{a} \frac{1 + \mathrm{i}\frac{A_\mathrm{p}}{A} \tan\theta(\tau)}{1 + \mathrm{i}\frac{A}{A_\mathrm{p}} \tan\theta(\tau)}$$

$$= \omega \frac{\rho(T_H)C(T_H)}{A_\mathrm{p}} A^2 \frac{1 + tan^2\theta(\tau)}{1 + \left(\frac{A}{A_\mathrm{p}} \tan\theta(\tau)\right)^2} \left\{ i + \frac{1}{2} \left(\frac{A}{A_p} - \frac{A_p}{A}\right) \sin 2\theta(\tau) \right\} \quad \text{(A22)}$$

Acknowledgement

I would like to express my grateful gratitude to Prof. K. Watanabe in faculty engineering of Hosei University and Prof. K. Kobayashi in faculty engineering of Hosei University for their guidance and numerous suggestions. I would like to thank for Prof. K. Suzuki in faculty engineering of Hosei University, who examined my doctor's degree and gave me precious opinions.

On writing individual paper, many people gave much support to me. Primarily, Prof. K. Watanabe's meticulous comments were an enormous help to me when I analyzed the sensing system.

Further, I wish to thank the assistance of the following students of Kobayashi Laboratory, Hosei University.

I wish finally to pay tribute to my parents for their support in many ways to this work.

March 24th, 2018
Tomoya Yoshida

Author

Tomoya YOSHIDA

March, 2013 Faculty of Science and Engineering, Hosei University
Bachelor of Electrical and Electronic Engineering

March, 2015 Graduate school of Science and Engineering, Hosei University
Major in Systems Engineering (Master's Program)

March, 2018 Graduate school of Science and Engineering, Hosei University
Major in Systems Engineering (Doctoral Program)